This is a repository copy of *DEM numerical investigation of wet particle flow behaviors in multiple-spout fluidized beds*.

Accepted Manuscript

DEM numerical investigation of wet particle flow behaviors in multiple-spout fluidized beds

Tianqi Tang, Yurong He, Tong Tai, Dongsheng Wen
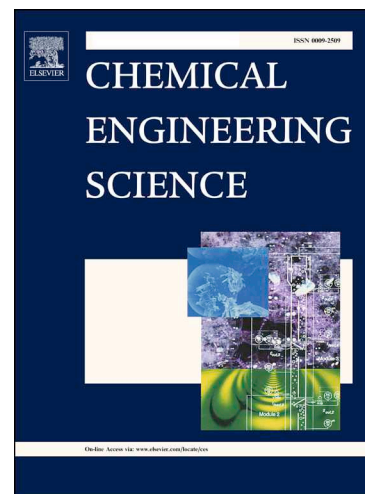
Please cite this article as: T. Tang, Y. He, T. Tai, D. Wen, DEM numerical investigation of wet particle flow behaviors in multiple-spout fluidized beds, *Chemical Engineering Science* (2017), doi: http://dx.doi.org/10.1016/j.ces. 2017.06.025

DEM numerical investigation of wet particle flow behaviors in multiple-spout fluidized beds

Tianqi Tang[1], Yurong He[1]*, Tong Tai[1], Dongsheng Wen[2, 3]

1 School of Energy Science and Engineering, Harbin Institute of Technology, Harbin 150001, China

2 School of Aeronautical Science and Engineering, Beihang University, Beijing 100000, China

3 Institute of Chemical and Process Engineering, University of Leeds, Leeds LS2 9JT, UK

Abstract: Spout fluidized beds are important for industrial processing, and multiple-spout fluidized beds play an important role in chemical reactions. However, particle flow behaviors in multiple-spout fluidized beds are not well known in wet particle systems. In this study, the flow behaviors of particles were investigated in dry and humid multiple-spout fluidized beds using a discrete element method (DEM). The simulated spout fluidized beds are similar to the ones used in the Buijtenen et al.'s experiment (published in Chemical Engineering Science, 2011, 66(11): 2368-2376). In the reference, particle flow behaviors were measured and investigated by PIV and PEPT in multiple spout fluidized beds. In this work, the simulated results are compared with the experimental data in single and double spout fluidized beds from Buijtenen et al., and the time-averaged particle velocities are compared to validate the simulation method. In contrast, simulated results with a liquid content of 1% in the bed showed good agreement with the data in the experimental results with an air relative humidity of 50%. Different liquid contents of the particles were applied to investigate the particle flow behaviors in wet granular systems. The liquid bridge force had a strong influence on the flow behaviors of the particles in the dense region, which resulted in different hydrodynamic characteristics between the dry and wet particles. In addition, the drag force dominated the particle flow behavior in the dry and wet particle systems. Moreover, in a wet granular system, the mass particle fluxes decreased, and the fluctuation of the pressure drops increased with an increasing influence of the liquid bridge force on the particles. Furthermore, with an increasing liquid content, the energy fluctuation of the particles and bubbles weakened gradually with less active motions. A comparison of the hydrodynamic flow behaviors in single-spout and double-spout fluidized beds was carried out as well. Comparisons of the solid circulation rate and the colliding characteristics between single-spout and double-spout fluidized beds were conducted. Particularly, a comparison of the mixing characteristics demonstrated that the particles were mixed more completely in a double-spout fluidized bed. Therefore, the double-spout fluidized bed could provide more adequate space for mass and heat transfer under the same condition. This was important in providing a theory for designing the industrial reactor.

Keywords: multiple-spout fluidized bed, wet particles, discrete element method, flow characteristics

1 Introduction

Spouted beds have gained increased recognition in recent years. They have been widely used for the production of particles through granulation, and they have been applied in the production of detergents, pharmaceuticals, food, and fertilizers[2]. The unique advantages, including enhanced heat and mass transfer rates and the high mixing rates of the particles[3], has initiated more

investigations of spouted fluidized beds. To overcome the limitation of the conventional single spouted bed, it has been modified for the purpose of optimum operation to yield various types of beds including slot-rectangular spout bed, spout bed with a draft tube, and multiple-spout bed. Owing to its high flexibility, easy design, and construction simplicity, the multiple-spout bed is promising for scaling-up. Besides, for industrial production, the scale of multiple-spout fluidized beds is essential to apply adequate space for mass and heat transfer between the particles. However, the investigations mainly focused on single-spout fluidized beds, and the gas-solid hydrodynamic characteristics in multiple-spout fluidized beds were not very clear. Thus, the flow behaviors of the particles in a multiple-spout fluidized bed require further study.

The spout fluidized bed involves complex gas-solid two-phase flow behaviors. A wide range of operating conditions results in various fluidization states. Some researchers have investigated the flow behaviors in spouted beds. For experiments, Buijtenen et al. (2011) investigated the collision properties of particles in a spout fluidized bed combining particle image velocimetry and digital image analysis. Luo et al. (2013) investigated solid dispersion and circulation properties in a 3D spouted bed with or without a draft tube. In addition, pressure drop fluctuation characteristics were researched by Duarte et al. (2009), Filia et al. (1983) and Zhong et al. (2005) for further understanding of the fluidization conditions in a spout fluidized bed. In a simulated analysis, Link et al. (2004) investigated the flow behaviors of particles in a spout fluidized bed using a hard sphere discrete particle model. In addition, Kawaguchi et al. (2002) and Zhang et al. (2010) revealed mixing and flowing mechanisms in an incline-bottomed and flat-bottomed spouted bed, respectively. With regard to the multiple-spout fluidized bed, Yang et al. (2014) tracked millions of particles by the parallel CFD-DEM coupling method, which is meaningful for the industrial processing. Ded et al. (2014) predicted the bubble characteristics in the fluidized bed with multiple jets. Wang et al. (2015) analyzed the mixing and segregation characteristics in a double spout fluidized bed. Besides, Saidi et al. (2015) investigated the gas-solid behaviors in the rectangular bed. As mentioned above, there have been a satisfactory number of experimental and simulated investigations on particle flow behaviors in spout fluidized beds. However, most of them are limited to the single-spout fluidized bed and double-spout fluidized bed, of which the latter system does not involve a cohesive liquid.

In fact, the presence of liquid is not neglected during industrial processing, such as a granular drying process in a spout fluidized bed (Zielinska et al., 2007; Khadilkar et al., 2014). Additionally, the particle flow characteristics change owing to the effect of the cohesive liquid between the particles (Liao et al., 2016; Chou et al., 2011). Further understanding of the flow behaviors of the particles in a wet granular system is necessary and essential, especially in a double-spout fluidzied bed. This is not present in previous investigations.

Experiments are essential for investigating the gas-solid hydrodynamic characteristics; however, the results are limited to macro-motion parameters, including particle velocity and pressure drop. Thus, with the development of computational fluid dynamics, the simulation of multi-phase flow behaviors has become an effective way to further investigate the gas-solid hydrodynamic characteristics in a gas fluidized bed. Pain et al. (2001) and Lu et al. (2009) have researched gas-solid flow using a two-fluid model (TFM). However, the TFM was used in an industrial scale, and the motion of an individual particle could not be captured. In addition, Wang et al. (2009) proposed that the TFM failed to predict the bed expansion in fluidized beds. Therefore, a discrete element method (DEM) is widely used to calculate and capture gas-solid

flow characteristics. For an in-depth study on particle systems, a modified soft sphere model was used, which was improved by Tsuji et al. (1993) based on the model proposed by Cundall and Strack (1979). The DEM has been widely used in inclined channels (Chang et al., 2008; Teufelsbauer et al., 2011), rotating drums (Xu et al., 2010; Arntz et al., 2008), and fluidized beds (Jia et al., 2015; Zhuang et al., 2014). Furthermore, gas and particle motions were captured and well analyzed. A few researchers also conducted investigations on spout fluizied beds using the DEM. For example, Limtrakul et al. (2004) and Zhao et al. (2008) used the DEM to predict the particle dynamics in spout fluidized beds. In addition, Jajcevic et al. (2013) investigated the particle flow characteristics in a multi-spout fluidized bed using the DEM. However, most of the simulations were limited to dry granular systems.

Researchers have investigated gas-solid two-phase flow in a dry particle system; however, little research has been conducted for multi-spout fluidized beds with a cohesive liquid. Thus, further investigation on the effect of the liquid contents of the particles on the gas-solid hydrodynamic characteristics in multi-spout fluidized beds is necessary. In this study, the effect of the liquid content on the gas-solid flow characteristics in single-spout and double-spout fluidized beds was conducted using a modified DEM. The organization of this study is as follows. A DEM combining the liquid bridge module was established to investigate the flow behaviors of particles in a multi-spout fluidized bed. A comparison between the simulated results and the experimental data was carried out in consideration of the relative humidity (RH). First, a force analysis of the wet particles was conducted. Subsequently, the hydrodynamic characteristics of the dry and wet particles were compared, and the effect of the liquid contents on the particle motions was investigated. In addition, a comparison of the gas-solid flow characteristics in single and double spouted fluidized beds was conducted with cohesive liquid.

Nomenclature

C	granular temperature [$m^2\ s^{-2}$]	**Subscript**	
d_p	particle diameter [m]	avg	average
DEM	discrete element method	A	area
$\mathbf{F}_c$	contact force [N]	c	contact
$\mathbf{F}_{gp}$	drag force [N]	cell	cell numbers
$\mathbf{F}_{lb}$	liquid bridge force [N]	cp	capillary
$\mathbf{g}$	gravitational acceleration [$m\ s^{-2}$]	g	gas phase
H	distance between particles [m]	f	fraction
HSD	Hertzian Spring Dashpot	lb	liquid bridge
I_p	moment of inertia [$kg\ m^2$]	n	normal direction
k_n	spring stiffness [N m]	neg	negative
LSD	linear Spring Dashpot	p	solid phase
m_p	particle mass [kg]	r	relative parameter
M	mixing index [-]	t	tangential direction
N	numbers [-]	Greek letter	
PEPT	positron emission particle tracking	β	interphase momentum exchange coefficient [-]
PIV	particle image velocimetry	γ	surface tension [$N\ m^{-1}$]
$\mathbf{r}_p$	the position of particle center [m]	δ	elastic deformation [m]
R	particle radius [m]	ε	volume fraction [-]
Re	Reynolds number [-]	θ	contact angle [rad]
t	time [s]	μ	friction coefficient [-]
$\mathbf{T}_p$	torque [N m]	ρ	density [$kg\ m^{-3}$]
$\mathbf{u}_g$	gas velocity [$m\ s^{-1}$]	σ	deviation [-]
$\mathbf{v}_p$	particle translational velocity [$m\ s^{-1}$]	τ	stress tensor [-]
V_{lb}	liquid bridge volume [m^3]	φ	half-filling angle [rad]
V_p	particle volume [m^3]	ω	rotational velocity [$rad\ s^{-1}$]

2 Model description

2.1 Gas phase

The gas phase was treated as a continuous phase and described by the Eulerian method. The mass and momentum equation were modeled by the local average Navier-Stokes equations proposed by Anderson and Jackson (1967), and the mass and momentum conservation equations are defined as follows:

$$\frac{\partial}{\partial t}\left(\varepsilon_g \rho_g\right) + \frac{\partial\left(\varepsilon_g \rho_g u_{g,i}\right)}{\partial x_i} = 0 \tag{1}$$

$$\frac{\partial}{\partial t}\left(\varepsilon_g \rho_g u_{g,i}\right) + \frac{\partial}{\partial x_j}\left(\varepsilon_g \rho_g u_{g,i} u_{g,j}\right) = -\varepsilon_g \frac{\partial p}{\partial x_i} + \frac{\partial}{\partial x_j}\left(\varepsilon_g \tau_{g,ij}\right) - F_{gp} + \varepsilon_g \rho_g g_i \tag{2}$$

where ε_g is the porosity, -; ρ_g is the density, $kg \cdot m^{-3}$; u_g is the gas velocity, $m \cdot s^{-1}$; g is the gravitational acceleration, $m \cdot s^{-2}$; p is the pressure, $Pa \cdot s$, and τ_g is defined as,

$$\tau_{g,ij} = \mu\left(\frac{\partial u_{g,i}}{\partial x_j} + \frac{\partial u_{g,j}}{\partial x_i} - \frac{2}{3}\frac{\partial u_{g,k}}{\partial x_k}\delta_{ij}\right) \tag{3}$$

2.2 Solid phase

In the DEM, the solid phase is treated as a discrete phase, and the motion of the particles was solved by Newton's second law directly. The soft-sphere model was proposed by P. A. Cundall et al. (1979), and modified by Y. Tsuji et al. (1993)
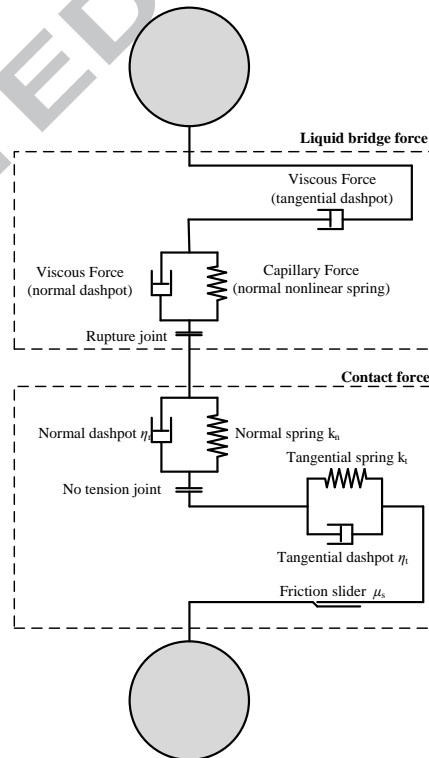

Fig. 1 Soft-sphere interaction model of wet cohesive particles

For translational motion, the particles are governed by four major forces, including the pressure gradient force, the drag force, the gravitational force, and the contact force between the colliding particles or the particles and the walls. In addition, the liquid bridge force was

considered in the wet system. For tracking the particle motion, a suitable time step should be well set to capture the particle flow behaviors during collision. The particle flow condition will update in every time step. Tsuji et al. mention that particles are governed by the sum of forces acting on the particle, including contact force and fluid forces.

$$m_p \frac{d^2 \mathbf{r}}{dt^2} = -V_p \nabla p + \frac{V_p \beta}{1 - \varepsilon_g} \left(\mathbf{u}_g - \mathbf{v}_p \right) + m_p \mathbf{g} + \mathbf{F}_c + \mathbf{F}_{lb} \tag{4}$$

where m_p is the particle mass, kg; $\mathbf{r}$ is the position of the particle center, m; t is the time, s; V_p is the particle volume, m^3; the $\mathbf{v}_p$ is the particle velocity, $m \cdot s^{-1}$; $\mathbf{F}_c$ is the contact force, N, and $\mathbf{F}_{lb}$ is the liquid bridge force, N.

For rotational motion, the angular velocity driven by the torque was given as follows:

$$I_p \frac{d\boldsymbol{\omega}_p}{dt} = \mathbf{T}_p = \mathbf{r}_p \times \mathbf{F}_t = \mathbf{r}_p \times (\mathbf{F}_{c,t} + \mathbf{F}_{lb,t}) \tag{5}$$

where I_p is the moment of inertia, $kg \cdot m^2$, and $\mathbf{T}_p$ is the torque, $N \cdot m$, $\mathbf{F}_t$ is generated by the contact force and the liquid bridge force in the tangential direction, as shown in Fig. 1. In the latest investigations, the rolling friction torque is taken account into the particle motion. In this paper, the rolling friction model (Zhou et al, 1993; Wang et al., 2014; Hosn et al., 2017) is neglected, which will be studied in the future investigations.

2.2.1 Contact force

As shown in Fig. 1, a linear spring-dashpot (LSD) soft-sphere model was applied to compute the contact force when a particle collided with another particle or a wall. Compared with the Hertzian (Gidapow, 1994) and Hertzian spring-dashpot (HSD) models (Johnson, 1985), the LSD model is commonly used because of the analytic relationships between the model inputs and desired properties such as the restitution coefficient and collision time. In addition, the LSD model is computationally more efficient because nonlinear operations need not to perform for each contact. Thus, the LSD soft-sphere model was employed in this work. (Morris et al., 2016)

The contact force was divided into two directions: the normal component and tangential component, which are described as follows:

$$\mathbf{F}_n = -k_n \boldsymbol{\delta}_n - \eta_n \mathbf{v}_n \tag{6}$$

$$\mathbf{F}_t = \begin{cases} -k_t \boldsymbol{\delta}_t - \eta_t \mathbf{v}_t & |\mathbf{F}_t| \leq \mu_f |\mathbf{F}_n| \\ -\mu_f |\mathbf{F}_n| \dfrac{\mathbf{v}_t}{|\mathbf{v}_t|} & |\mathbf{F}_t| > \mu_f |\mathbf{F}_n| \end{cases} \tag{7}$$

where k is the spring stiffness, $N \cdot m^{-1}$; δ is the elastic deformation, m; $\mathbf{v}_r$ is the relative velocity, $m \cdot s^{-1}$, μ_f is the coefficient of sliding friction, -. According to the expression, the elastic deformation and damping effect were described by the position-dependent spring obeying Hooke's law and the velocity-dependent dashpot, respectively.

2.2.2 Liquid bridge force

The liquid bridge force was proposed for a wet system. Girardi et al. (2016) investigated the cohesive liquid bridge force in a gas–solid fluidized bed while considering the capillary force only. In this work, both the capillary and viscous forces are considered.

Based on a traditional model, the liquid bridge force is added to investigate the influence on the collisions between the particles or the particles and walls. The liquid bridge force consists of a

capillary force and a viscous force. Fig. 2 shows the structure of the liquid bridge under different conditions.

(a) particle-particle   (b) particle-wall

Fig. 2 Schematic of liquid bridge between particles
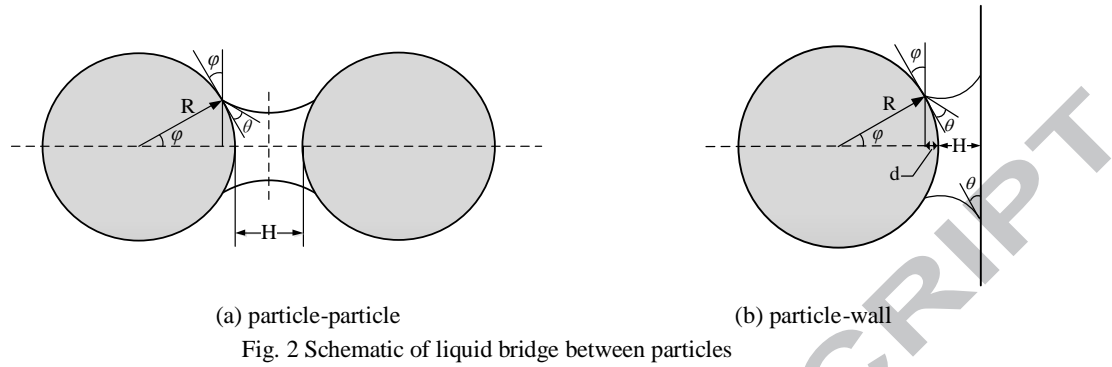
2.2.2.1 Capillary force

For particle-particle interaction, according to a total energy theory (Israelachvili et al., 1992), the capillary force of a fixed liquid volume was calculated. The expression is shown below.

$$F_{cp,n} = -\frac{2\pi\gamma R\cos\theta}{H/2d+1} - 2\pi\gamma R\sin\varphi\sin(\varphi+\theta) \tag{8}$$

where γ is the surface tension, N·m^{-1}; R is the particles radius, m; φ is the half-filling angle, rad; θ is the contact angle, rad; H is the distance between the two particles, m, and d is the immersion height, m, which is defined as $d = R - R\cos(\varphi)$.

Similar to the interaction between particles, the capillary force between a particle and a wall was expressed as follows:

$$F_{cp,n} = -\frac{4\pi\gamma R\cos\theta}{H/d+1} - 2\pi\gamma R\sin\varphi\sin(\varphi+\theta) \tag{9}$$

In Equation (8), H represents the distance between the particles. The value of H is negative when particles overlap, which does not correspond to a real physical process. Thus, the minimum value of H was set as 10^{-5} m to ensure that the normal capillary force was positive. The setting of the minimum value was also suitable for calculating the normal viscous force.

2.2.2.2 Viscous force

Viscous force is as important as capillary force. Generally, the capillary force is dominant. However, the viscous force becomes more effective when the liquid viscosity or relative velocity was higher than usual. Based on the lubrication theory (Bird et al., 1960) and the work of Adams and Edmonson (1987), the normal component was given as

$$F_{v,n} = 6\pi\mu_{lb}Rv_{r,n}\frac{R}{H} \tag{10}$$

The parameter μ_{lb} is the liquid viscosity, Pa·s.

The viscous force in the tangential direction was solved by Lian et al. (1996) and was defined as,

$$F_{v,t} = 6\pi\mu_{lb}Rv_{r,t}\left(\frac{8}{15}\ln\frac{R}{H}+0.9588\right) \tag{11}$$

Furthermore, the critical rupture distance H_{cr} is an important parameter for the calculation of the liquid bridge force. When the distance between particles or a particle and a wall was larger

than H_{cr}, the liquid bridge ruptured. The relationship between H_{cr} and the liquid bridge volume was proposed by Lian (1993) and defined as:

$$H_{cr} = R(0.5\theta + 1)\sqrt[3]{\hat{V}_{lb}} \tag{12}$$

Here, $\hat{V}_{lb}$ is the dimensionless liquid bridge volume and is defined below:

$$\hat{V}_{lb} = \frac{V_{lb}}{R^3} \tag{13}$$

2.3 Interphase exchange

The momentum exchange between the gas and solid phase has been studied. As a function of the product of the interphase momentum exchange coefficient and the relative velocities of the two phases, the rate of momentum exchange F_{gp} between the solid and gas phase was composed of the sum of the drag forces acting on the individual particles in a computing cell. Following Anderson and Jackson (1967) and Pritchett et al. (1987), F_{gp} can be defined as the modified format, and shown as Equation (14):

$$F_{gp} = \frac{1}{V_{cell}} \sum_{k=1}^{n} \frac{V_p \beta}{1 - \varepsilon_g} \left(u_g - v_p^k \right) \tag{14}$$

The interphase momentum exchange coefficient β depended strongly on the local void fraction of the gas phase.

The drag force had an influence on the flow behaviors of a particle in the DEM simulation, which was indicated by Beetstra et al. (2007). The Beetstra drag force model, derived from lattice-Boltzmann simulations, was justified for a Reynolds number of up to 1000, which was the range of the Re in the Koch-Hill et al. (2001) drag force model. According to Beetstra et al., it can be written as,

$$\beta_{Beetstra} = K_1 \mu \frac{\left(1 - \varepsilon_g\right)^2}{d_p^2 \varepsilon_g} + K_2 \mu \frac{\left(1 - \varepsilon_g\right) Re}{d_p^2} \tag{15}$$

$$K_1 = 180 + 18 \frac{\varepsilon_g^4}{1 - \varepsilon_g}(1 + 1.5\sqrt{1 - \varepsilon_g}) \tag{16}$$

$$K_2 = 0.31 \frac{\varepsilon_g^{-1} + 3\varepsilon_g(1 - \varepsilon_g) + 8.4 Re^{-0.343}}{1 + 10^{3(1-\varepsilon_g)} Re^{2\varepsilon_g - 2.5}} \tag{17}$$

The Re for the solid phase was defined as,

$$Re = \frac{\rho_g \varepsilon_g d_p |u_g - v_p|}{\mu} \tag{18}$$

In this work, the effect of the drag force model on particle flow behaviors is compared. Additionally, the Koch–Hill et al. (2001) model and Gidaspow et al. (1994) models are also applied, which are defined as follows,

$$\beta_{Koch-Hill} = \frac{18\mu_g \varepsilon_g^2 \varepsilon_p}{d_p^2} \left[F_0\left(\varepsilon_p\right) + \frac{1}{2} F_3\left(\varepsilon_p\right) Re \right] \tag{19}$$

$$F_0\left(\varepsilon_p\right) = \begin{cases} \dfrac{1+3\sqrt{\dfrac{\varepsilon_p}{2}}+\dfrac{135}{64}\varepsilon_p \ln\left(\varepsilon_p\right)+16.14\varepsilon_p}{1+0.681\varepsilon_p-8.48\varepsilon_p^2+8.16\varepsilon_p^3} & \varepsilon_p < 0.4 \\[4mm] \dfrac{10\varepsilon_p}{\varepsilon_g^3} & \varepsilon_p \geq 0.4 \end{cases} \tag{20}$$

$$F_3\left(\varepsilon_p\right) = 0.0673 + 0.212\varepsilon_p + \frac{0.0232}{\varepsilon_g^5} \tag{21}$$

Gidaspow et al. (1994) models is defined as Equation (22) shown,

$$\beta_{\text{Gidaspow}} = \begin{cases} \dfrac{150\left(1-\varepsilon_g\right)^2 \mu_g}{\varepsilon_g d_p^2} + 1.75\dfrac{\rho_g\left(1-\varepsilon_g\right)}{d_p}\left|\mathbf{u}_g-\mathbf{v}_p\right| & \varepsilon < 0.8 \\[4mm] \dfrac{3}{4}C_D \dfrac{\rho_g\left(1-\varepsilon_g\right)\varepsilon_g^{-1.65}}{d_p}\left|\mathbf{u}_g-\mathbf{v}_p\right| & \varepsilon > 0.8 \end{cases} \tag{22}$$

where C_D is defined as follows,

$$C_D = \begin{cases} \dfrac{24}{\text{Re}}\left(1+0.15\,\text{Re}^{0.687}\right) & \text{Re} < 1000 \\[2mm] 0.44 & \text{Re} \geq 1000 \end{cases} \tag{23}$$

2.4 Granular temperature

The granular temperature, based on the random fluctuation of particle velocity, is one of the most important parameters for measuring the kinetic behavior in particulate systems. Tartan and Gidaspow (2004) and Jung et al. (2005) proposed two granular temperatures owing to different oscillations of the particles. The first was a granular temperature caused by oscillations of the particles. The second was a bubble granular temperature caused by the formations and motions of the clusters. In this study, the particle flow behaviors are investigated in a spouted fluidized bed. Thus, the bubble granular temperature was not considered or analyzed due to no obvious bubble phenomenon.

2.4.1 Particle granular temperature

The granular temperature is determined by the second moment of particle velocity fluctuation, which was expressed as,

$$\left\langle C_i C_j \right\rangle(r,t) = \frac{1}{n}\sum_{k=1}^{N_p}\left[v_{p,i}^k(r,t)-c_i(r,t)\right]\left[v_{p,j}^k(r,t)-c_j(r,t)\right] \tag{24}$$

where N_p is the number of particles in a cell, and i is the direction. The cell-average mean velocity c was defined as

$$\left\langle C_i C_j \right\rangle(r,t) = \frac{1}{n}\sum_{k=1}^{N_p}\left[v_{p,i}^k(r,t)-c_i(r,t)\right]\left[v_{p,j}^k(r,t)-c_j(r,t)\right] \tag{25}$$

The particle granular temperature was defined as,

$$\theta_p\left(\mathbf{r},t\right) = \frac{1}{3}\left\langle C_x C_x\right\rangle\left\langle r,t\right\rangle + \frac{1}{3}\left\langle C_y C_y\right\rangle\left\langle r,t\right\rangle + \frac{1}{3}\left\langle C_z C_z\right\rangle\left\langle r,t\right\rangle \tag{26}$$
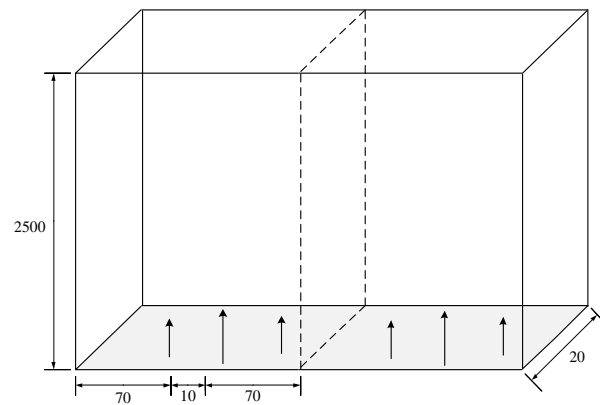
2.5 Boundary conditions

Fig. 3 Structure of a multi-spout fluidized bed

In this study, the particle flow behavior with and without cohesive liquid were performed in single and double spout fluidized beds. As shown in Fig. 3, the bed structure was the same as the experimental structure of Buijtenen et al.(2011) Based on the reference, the sizes of single and double spouted fluidized beds are $150 \times 20 \times 2500$ mm and $300 \times 20 \times 2500$ mm, respectively. The double-spout fluidized bed could be treated as two single-spout fluidized beds connected through the dash baffles. At the bottom of each single-spout fluidized bed, the fluidizing gas entered through three independent sections: two 70-mm wide fluidizing regions at the sides and one 10-mm wide spouting region at the center. The gas velocities for the spouting and fluidizing region are shown in Table 1. Besides, the particle flow behaviors were measured by PIV and PEPT, and the differences between the two methods were compared. In this work, the simulated results are compared with the experimental data for single and double spout fluidized beds reported by Buijtenen et al. (2011) The time-averaged particle velocity was compared in consideration of the relative air humidity. In this study, all the experimental environment effects are taken into account, and the simulation model and results are verified and validated in the following sections. Furthermore, the grid size and number of particles shown in Table 1 are selected based on the experimental setting. (Buijtenen et al., 2011) The gird sizes are $15 \times 2 \times 250$ and $30 \times 2 \times 250$ for the single and double spouted fluidized beds, respectively. According to the mesh independence test, the grid sizes adopted in this work were sufficient to obtain accurate results. For the gas phase, a pressure outlet boundary condition was applied to the top outlet of the bed and a no-slip boundary condition was adopted at the walls.

2.6 Numerical procedure

A modified multiphase flow with interphase exchanges (MFIX) DEM code, developed at National Energy Technology Laboratory (NETL), was used for the simulations in this study. In the numerical simulation, the hydrodynamic equations of the gas phase were solved with a finite volume method and a discretization on a staggered grid. All of the simulations of the dry and wet granular systems were carried out for 15 s, and the time-averaged results were obtained from the last 10 s. In the simulations, uniform glass spherical particles with a diameter of 3 mm and a density of 2505 kg/m^3 were used. The physical properties and particle collision parameters, based on the experimental parameters and the theoretical value proposed by Kuo et al. (2002), are summarized in Table 2.

For the numerical simulation, time and space discretization setting is important for obtaining accurate simulation results. (Guédon et al., 2017) In contrast, a DEM method is applied in this paper. Particles are treated as discrete phase, and solved by Newton's second law in a time step. In the soft-sphere model, deformation is allowed at the contact point between a particle and another particle or a wall. In general, the contact and liquid bridge forces were higher than the gravitational force as demonstrated in Section 3.4. Thus, an extra time step was set to capture and describe the effect of the contact and liquid bridge forces. The time step is 2×10^{-5}s. For the gas phase, the flow behaviors were discretized in a staggered grid and solved by the finite volume method. Mesh size applied is shown in Table 1. Moreover, it is crucial to consider CPU-time consumption while calculating particle flow behaviors by DEM method. CPU-time is an important parameter to reflect the calculation efficiency, and is mainly spent on calculating particle collisions. Thus, it is observed that more time is taken with an increasing of particle number. The CPU time required for the calculation of 10s is approximately 330h for the single spout fluidized bed and 770h for the double spout fluidized bed on a personal computer (8 cores, 30 GHz), respectively.

Table 1 Numerical settings

	U_{sp} (m/s)	U_{bg} (m/s)	N_p	N_x	N_y	N_z
Single-spout	43.5	2.4	12000	15	2	250
Double-spout	40.5	2.4	48000	30	2	250

Table 2 Parameters applied in the simulation

VARIABLE	VALUE	UNIT
Particle		
Particle diameter, d_p	3.00	mm
Particle density, ρ_p	2505	kg/m^3
Coefficient of restitution, e	0.97	-
Coefficient of sliding friction, $\mu_{f,p-p}$	0.10	-
Coefficient of sliding friction, $\mu_{f,p-w'}$	0.30	-
Normal spring stiffness, k_n	1000	N/m
Tangential spring stiffness, k_t	286	N/m
Gas		
Density, ρ_g	1.2	kg/m^3
Viscosity, μ	1.8×10^{-5}	Pa·s
Outlet pressure, P	1.2×10^{5}	Pa
Liquid		
Relative liquid volume, V_{lb}^{*}	0.01%, 0.10%, 1.00%	-
Liquid viscosity, μ_{lb}	1.03×10^{-3}	Pa·s
Contact angle, θ	30	Deg
Surface tension, γ	0.0721	N/m

3 Results and discussion

3.1 Model validation and verification

3.1.1 Model verification

3.1.1.1 Verification of mesh size

Table 3 Gird numbers applied for the mesh independence

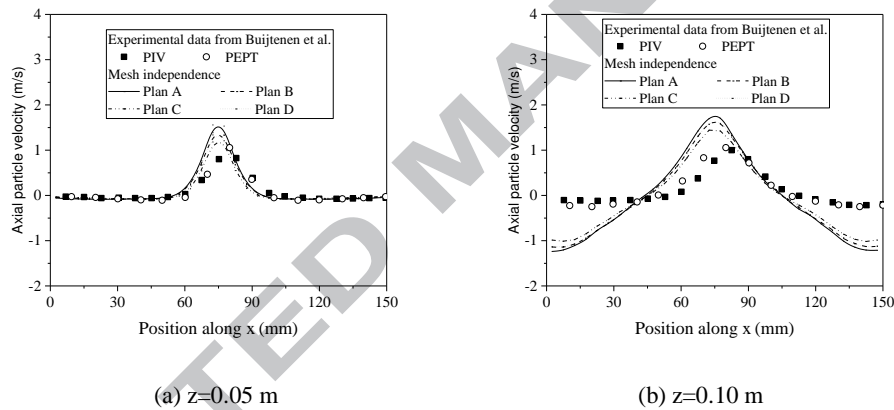|	Grid number (-)	Grid size (mm)
Plan A	15×3×250	10×6.6×10
Plan B	15×2×275	10×10×9.09
Plan C	15×2×250	10×10×10
Plan D	15×2×200	10×10×12.5

(a) z=0.05 m   (b) z=0.10 m

Fig. 4 Profiles of time-averaged vertical particle velocities in single spout fluidized beds

In numerical simulations, the number of grids might influence the simulation results. To verify the mesh independence and study the effect of the grid numbers on the simulations, four plans are considered in this work. The grid number in Plan C is that adopted in the simulation. The grid size and number are applied in Table 3. Fig. 4 presents the axial particle velocity distributions obtained for the different plans. The results of the four plans are close to each other, except near the wall where the axial particle velocities for Plan C agree best with the experimental results, followed by Plans D, A, and B. In conclusion, the grid numbers are not reasonable to obtain high-accuracy results with an extremely large or extremely small cell size. Therefore, the grid size in Plan C is applied for the accuracy of the simulation results and saving computational time in this work.

3.1.1.2 Verification of drag force model

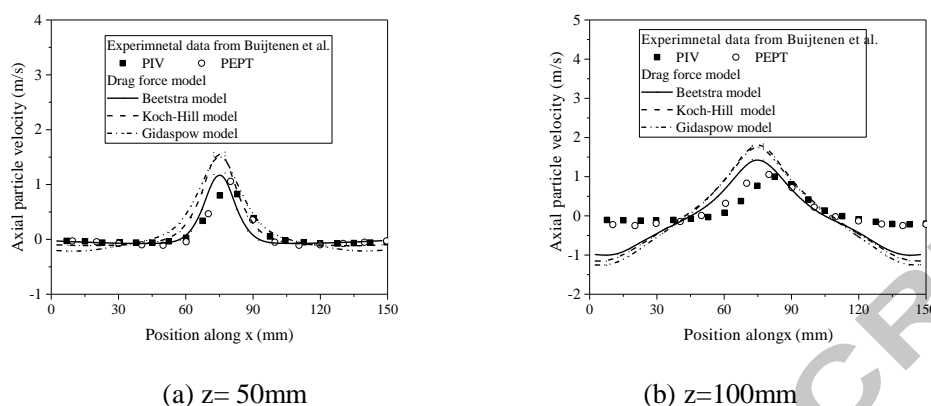(a) z= 50mm   (b) z=100mm

Fig. 5 Influence of drag force models on axial particle velocity

The drag model is critical to the simulation of two-phase gas–solid flows. To choose a suitable drag model, the effect of drag models on axial particle velocities was compared. From Fig. 5, it can be obtained that the distribution of axial particle velocity is influenced by drag force model. It is obvious to obtain that the particle velocity of particle velocity agree with the experimental data with the Beetstra drag force model, particularly in the spout region. In addition, the Beetstra drag force model, derived from lattice-Boltzmann simulations, was justified for a Re up to 1000, which was in the range of the Re in the Koch–Hill drag force model. Furthermore, Jajcevic et al. (2013) and Boyce et al. (2016) used the Beetstra drag force model to describe the interphase momentum in a spout fluidized bed and obtained ideal simulation results that exhibited a good agreement with the experimental data. Thus, the Beetstra drag model is applied in this work.

3.1.2 Model validation

To validate the simulation method, a comparison was carried out between the simulation results of this study and the experimental data from Buijtenen et al. (2011)
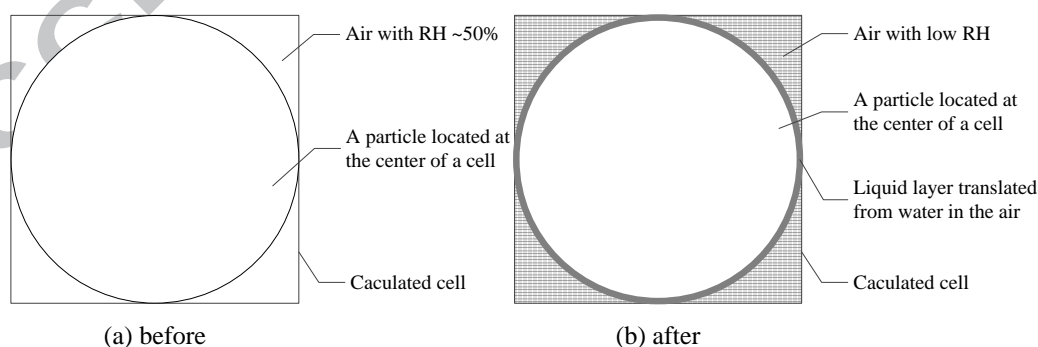

(a) before   (b) after

Fig. 6 Translation processing of relative liquid content from air to the surface of each particle

In general, the dry particle system is treated as an ideal environment without liquid, and the effect of air humidity is neglected. To prevent electrostatic charging of the particles, however, the background fluidization air was humidified to 50% RH in the experiment. Besides, parameters of

gas is set based on the dry air, and the air humidity is not considered. Thus, there was some deviation between the simulation setting and the experimental environment. We assumed that the liquid was generated by the air humidity. According to the thermodynamic calculation, the RH could be translated into the amount of liquid in the air, as shown in Fig. 6. Landi et al. (2011) proposed the relationship between the RH and the relative mass of the liquid and particle using a thermogravimetric analysis. The relative liquid content was defined as the ratio of the liquid volume to that of the particles. Therefore, according to the thermodynamic calculation and relative references, the amount of liquid was distributed equally on the surface of each particle. The simulated results with and without cohesive liquid were evaluated to explain the effect of air humidity and to validate the accuracy of the calculated model.
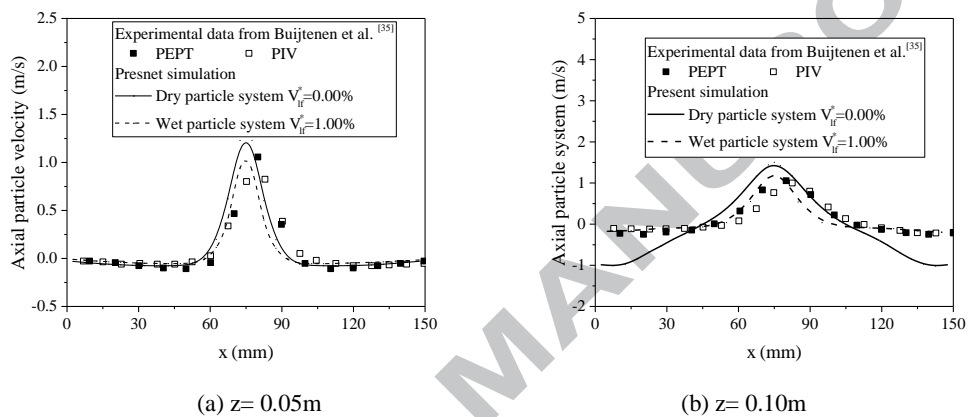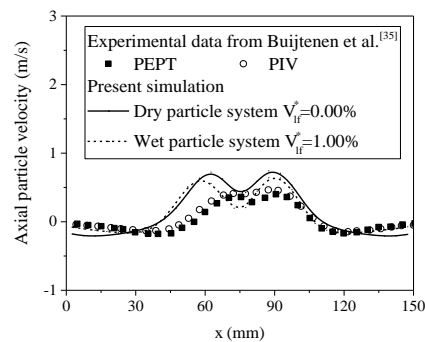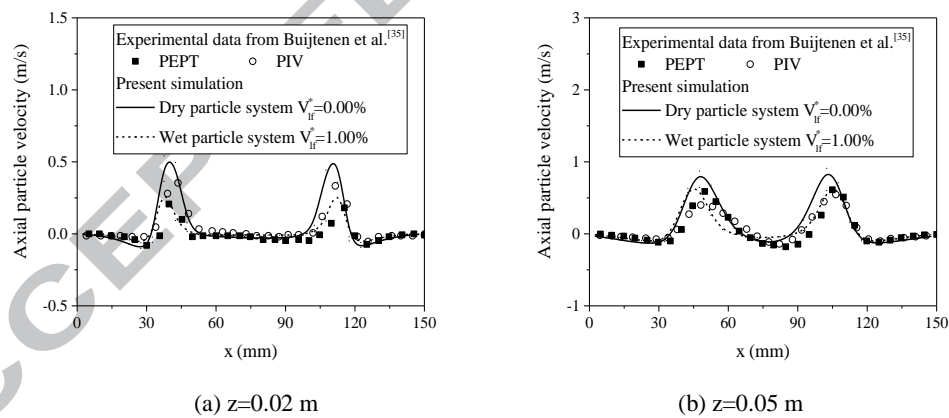
(a) z= 0.05m

(b) z= 0.10m

Fig. 7 Profiles of time-averaged vertical particle velocities in single spout fluidized beds

(a) z=0.02 m

(b) z=0.05 m

(c) z=0.10 m

Fig. 8 Profiles of time-averaged vertical particle velocities in double spout fluidized beds

A comparison between the simulation results in this study and the experimental results from Buijtenen et al. is shown in Figs. 7 and 8. For the experiments, Buijtenen et al. measured the particle velocities using the positron emission particle tracking (PEPT) method and particle image velocimetry (PIV). For single-spout and double-spout fluidized beds, particle velocities reached their peak value in the spout region. More particles were fluidized when the bed height increased. At a 100mm bed height in the double-spout fluidized bed, the particle velocities increased between the two gas inlet regions. The particle velocity was approximately zero near the walls. The profiles of the axial particle velocities contained a better agreement with the experimental data in the wet particle system than in the dry particle system, especially near the walls and spout regions. This demonstrated that the amount of water in the air cannot be neglected, and the flow behavior of the particles was influenced by the air humidity. For a single-spout fluidized bed, the axial particle velocity distributions at heights of 50 mm and 100 mm are compared with the experimental data. The results with a cohesive liquid has a better agreement with the experimental data. The importance of an investigation of wet particle flow behaviors was shown.

According to the model validation, it is obvious to find that the simulation results have a certain difference compared with the experimental data, especially in the dry granular system. According to the experimental environment proposed in the reference, the air humidity increased to 50% and can't be neglected in the numerical simulation. Thus, in this paper, the effect of air humidity is considered. The air humidity is converted into the relative liquid content. After transformation, the axial particle velocity more agrees with the experimental data with a little difference. Besides, it is obvious to obtain that the distribution of axial particle velocity data is asymmetric due to experimental system error. Moreover, the mathematical model is simplified suitably based on the actual colliding processing. Above all, the deviation is from both the simplified numerical model and experiment system.

Therefore, considering the amount of water in the air is necessary for evaluating particle flow behaviors. Meanwhile, the model used in this study was reasonable and accurate for investigating and capturing the flow characteristics of particles in dry and wet granular systems.

3.2 Pressure drop

Pressure drop is an important parameter for judging the fluidized condition in a gas-fluidized bed. The fluctuations of pressure drop periodically changed after 4 s, demonstrating that the particles were completely fluidized.

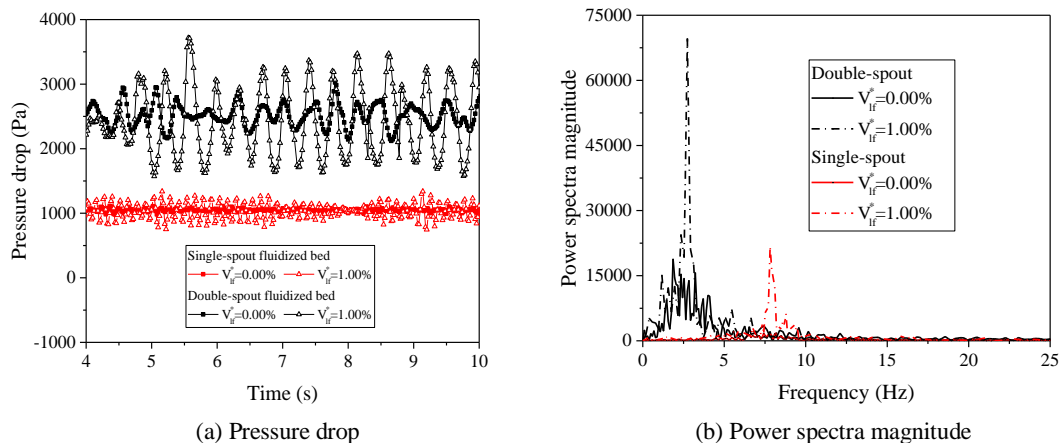
(a) Pressure drop   (b) Power spectra magnitude

Fig. 9 Influence of relative liquid volume on pressure drop and power spectra magnitude with multiple jets

Fig. 9 (a) shows the effect of the liquid content on the pressure drop as a function of time in single-spout and double-spout fluidized beds. The fluctuation of pressure drop waves and the average value decreased with increasing liquid content for both beds. For the single-spout fluidized bed in the dry granular system, the average value declined from 1050.47 Pa to 1033.88 Pa with a liquid content of 1.00%. For the double-spout fluidized bed in the dry granular system, the average value declined from 2512.82 Pa to 2429.21 Pa with the liquid content of 1.00%. However, the pressure drop of the wet particles was higher than that of the dry particles because the bubbles had to overcome the resistance from the particles before rising to the bed surface in a spout fluidized bed. In a wet particle system, the resistance was increased owing to the liquid bridge between the particles, and the decreasing average value demonstrated that the cohesive liquid influenced the gas motions. Thus, the fluctuation of the pressure drop was much higher with a decreasing average value in the wet particle system.

Fig. 9 (b) shows the distribution of power spectrum magnitude of the pressure drop using a fast Fourier transform method of for single-spouted and double-spouted fluidized beds with different liquid contents of the particles.

For both spouted fluidized beds with a different number of gas inlets, dominant peaks were observed in the wet particle systems, and the peak value increased sharply with a cohesive liquid. The dominant peaks were not obvious in the dry particle system. According to the distribution of the pressure drop, the pressure drop fluctuation was not significant in the dry particle system. However, the fluctuation of pressure drop increased and showed a more obvious periodic variation with a cohesive liquid. Thus, the existence of the dominant peak in the wet granular system was consistent with the profiles of the pressure drop.

By comparing the distributions of pressure drop and power spectra magnitude in single- and double-spouted fluidized beds, the fluctuation of pressure drop in a single-spout fluidized bed was more obvious than that in the double-spout fluidized bed because the number of particles in the single-spout fluidized bed was 25% of that in the double-spout fluidized bed. More particles were fluidized in the double-spout fluidized bed under a similar boundary condition. This resulted in a higher frequency of the solid circulation rate in a single-spout fluidized bed. Therefore, the dominant frequency in the single-spout fluidized bed was three times higher than that in the double-spout fluidized bed.

3.3 Analysis of the effect of liquid bridge force

In a wet granular system, the liquid bridge force and the contact force dominated the particle flow behaviors. To show the effect of the liquid bridge force on the flow behaviors of the particles, the ratio of the liquid bridge force to the contact force, as a function of the particle fraction, is shown in Fig. 10. The ratio distribution could be divided into three zones based on the range of the ratio as a function of the particle fraction. The flow behaviors were different in the single- and double-spout fluidized beds. The effect of the liquid bridge force was different in the related regions.

The effect of the liquid bridge force was obvious with particle fractions of 0 to 0.1 and 0 to 0.2 for the single-spout and double-spout fluidized beds, respectively.

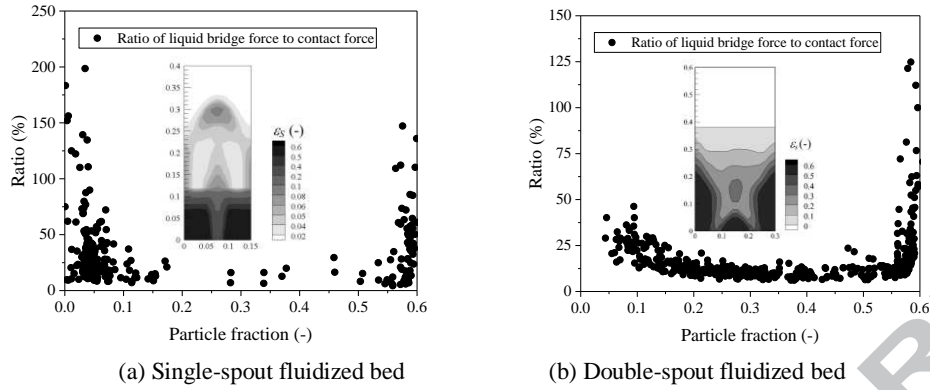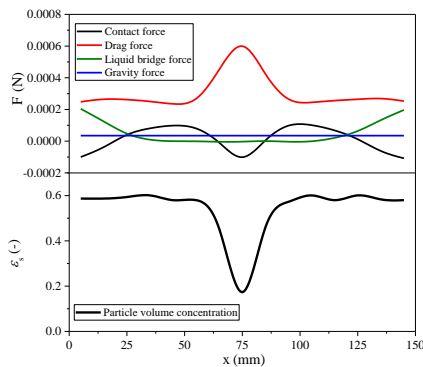(a) Single-spout fluidized bed (b) Double-spout fluidized bed

Fig. 10 Ratio of liquid bridge force to contact force as a function of particle fraction
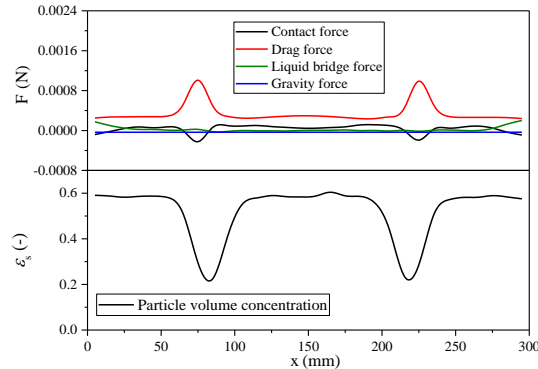
For the single-spout fluidized bed, particle fractions of 0 to 0.1 corresponded to the fountain region based on the cloud map. In the fountain region, particles were carried to the bed surface in agglomerates under the effect of the liquid bridge force. For the double-spout fluidized bed, particle fractions of 0 to 0.2 corresponded to the bed surface. In the dilute region, particles were pushed to both sides by bubbles and formed agglomerates under the effect of the liquid bridge force. Thus, the particle concentration was low owing to the liquid bridge force effect at the bed surface and fountain region.

The ratio was approximately 10 to 25% with a particle concentration less than 0.55. This particle concentration corresponded to the annulus regions with different numbers of jets, where particles were completely fluidized, and gas velocities were high. In this region, the liquid bridge force was less effective in dominating the particle motions; however, it cannot be neglected with a ratio of approximately 10 to 25%. Thus, particles were primarily governed by the contact force and secondarily governed by the liquid bridge force.

Near the walls and between the two gas-spouting regions for the double-spout fluidized bed, the particle concentration ranged from 0.55 to 0.6, where the effect of the liquid bridge force was more effective. With an increasing particle fraction, the particles were closer, and the effect of the liquid bridge force was more apparent. Furthermore, the contact and liquid bridge forces governed the particle flow behaviors together. In conjunction with the distribution of the particle mass flux, the particles moved downward slowly near the walls owing to an increase in the liquid bridge force. This phenomenon illustrated that the liquid bridge force dominated the particle motions in the dense regions. The existence of the liquid resulted in a strong difference in the particle flow behaviors.

(a) Single-spout fluidized bed (b) Double-spout fluidized bed

Fig. 11 Distributions of major forces and particle volume fraction in wet granular system

In the Fig. 10, the ratio of the liquid bridge force and the contact force was analyzed. To explain the effect of the liquid bridge force, a force analysis of the particles in the wet granular system was performed and is shown in Fig. 11. The force analysis provided detailed information for the particle flow behaviors with the effect of the governing force. The distribution of the particle volume fraction was shown as well. According to Equation (4), the particles were governed by the contact force, liquid bridge force, drag force, and pressure gradient force. Thus, the distribution of each force has been analyzed. According to the force profiles, the distribution of the forces was similar.

According to the Fig. 11, the drag force dominated the particle flow behaviors. The drag force reached the peak value in the spout region, where the gas velocity was high with a minimum particle volume concentration. It then decreased from the peak value to a minimum value near the walls at a high particle volume fraction. This phenomenon demonstrated that the drag force dominated the particle flow behaviors in a spout fluidized bed.

In the wet granular system, particle flow characteristics were influenced by the liquid bridge force according to the following profiles of the axial particle velocities and granular temperatures. The gravity force was a constant at 3.5×10^{-5} N. The maximum value of the liquid bridge force, appearing near the walls with a high particle concentration, was approximately 2.5×10^{-5} N. The maximum value was close to the drag force and nearly ten times and two times larger than the gravity force and contact force, respectively. Thus, near the walls, the liquid bridge force had the same effect on the particle flow behaviors. As the particle volume concentration declined from the walls to the middle spout region, the liquid bridge force decreased gradually. However, the contact force became more effective, which corresponded to the ratio distribution shown in Fig. 9. This indicated that the particles formed agglomerates near the walls with an effective liquid bridge force. In the spout region, particles were dominated and carried to the freeboard by the drag force. Particle agglomerations easily collided with each other, and the effect of the contact force was more evident than that of the liquid bridge force.

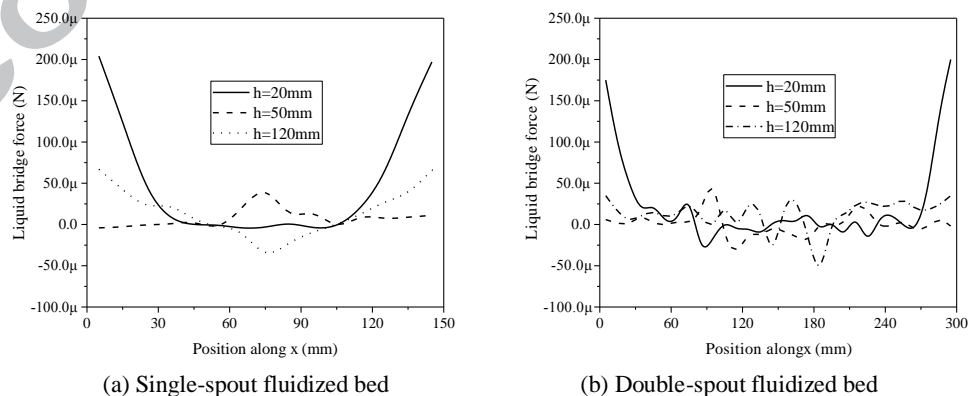(a) Single-spout fluidized bed   (b) Double-spout fluidized bed

Fig. 12 Distributions of liquid bridge force at different heights

Fig. 12 shows the distribution of liquid bridge at different heights in single and double spouted fluidized beds.

In a single-spout fluidized bed, the distribution of the liquid bridge force is symmetrical at a

bed height of 20 mm and it has a strong effect on the particle flow behavior. Near the walls, the liquid bridge force is approximately 250 μN, which is 10 times greater than the gravitational force. The liquid bridge force decreases gradually from both side walls to the gas inlet region. This indicates that particles forming dead zones at closer distance are a result of the effect of liquid bridge force that limits the particle flow behavior. Near the gas inlet region, particles are dominated by rapidly spouting gas directly, where the particle volume concentration is low. Thus, the liquid bridge force has a strong effect on the particle flow behavior, and it decreases gradually from both sides to the bed center at a bed height of 20 mm. With an increasing of bed height, the value of the liquid bridge force decreases gradually and then increases in the spout region. This is because the particles are fluidized completely with a marginal effect on the particle flow behavior, and they collide with each other under the effect of the liquid bridge force and drag force.

Compared with the single-spout fluidized bed, the distribution of the liquid bridge force is similar at a bed height of 20 mm in the double-spout fluidized bed. It is clearly seen that the distribution in a double-spout fluidized bed is more violent than that in the single-spout fluidized bed. This may be explained based on the fact that the particles are fluidized and mixed more completely with two gas inlets in the double-spout fluidized bed.

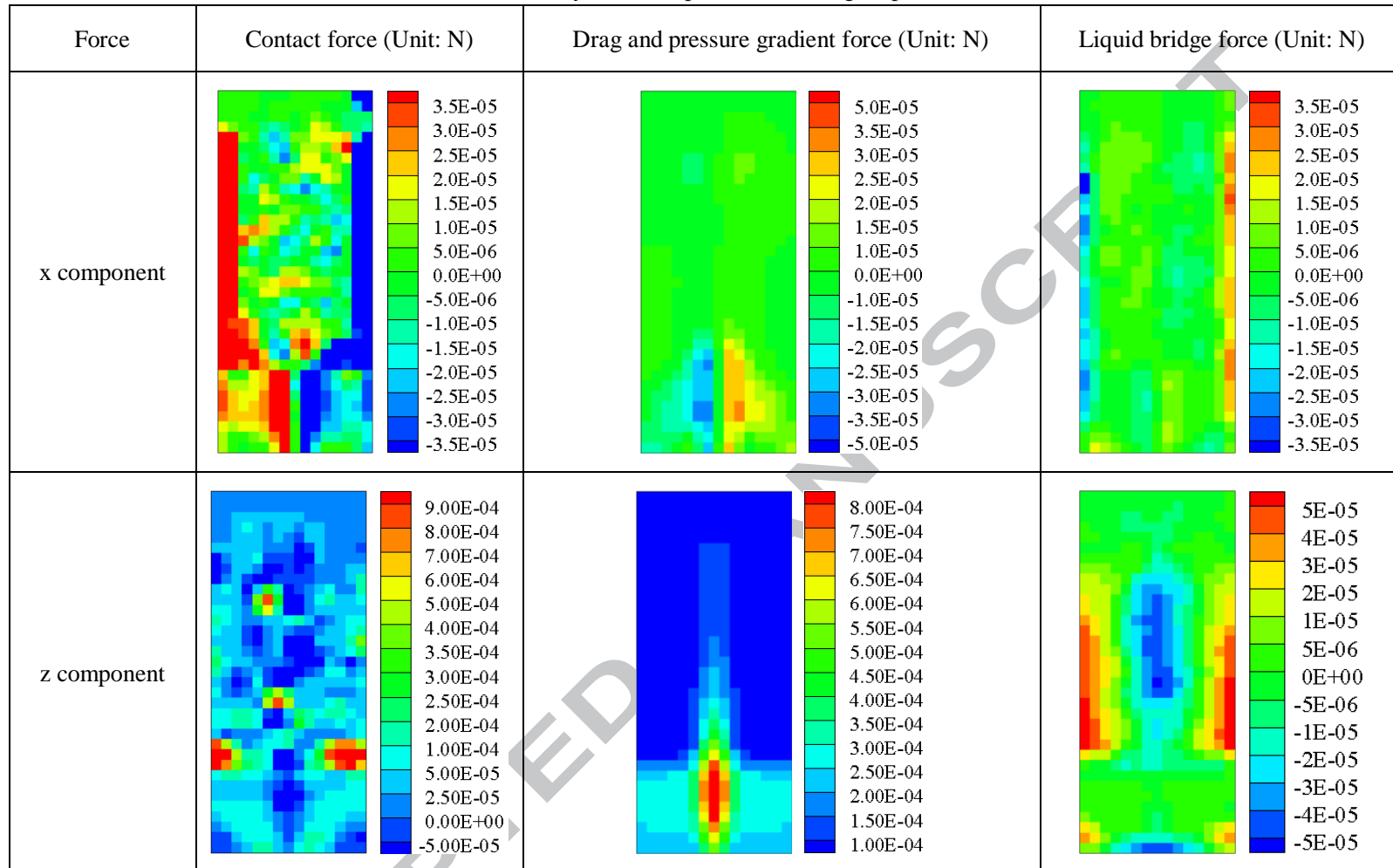Table 4 Force analysis of wet particles in a single-spout fluidized bed
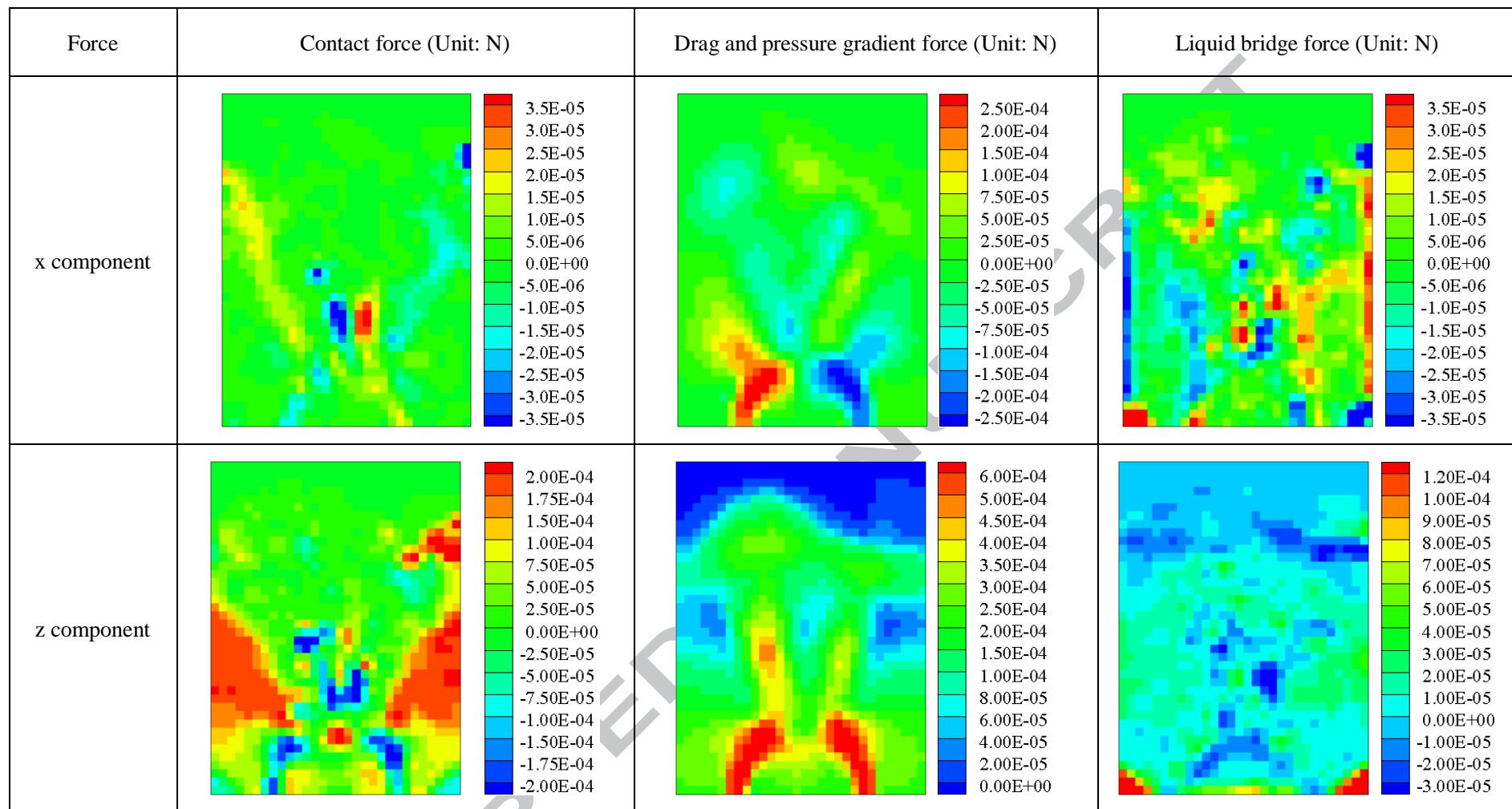
Force	Contact force (Unit: N)	Drag and pressure gradient force (Unit: N)	Liquid bridge force (Unit: N)
x component			
z component			

Table 5 Force analysis of wet particles in a double-spout fluidized bed

Force	Contact force (Unit: N)	Drag and pressure gradient force (Unit: N)	Liquid bridge force (Unit: N)
x component			
z component			

The cloud maps of the contact force, drag force, and liquid bridge force in the x-direction and z-direction are shown in Tables 4 and 5 for single-spout and double-spout fluidized beds, respectively. According to the cloud maps of force distribution, the magnitude of force in the x-direction was smaller than that in the z-direction for all governing forces.

The particles were mainly governed by the drag force, and the liquid bridge force influenced particle flow behaviors near the walls and dead zones in the wet granular system. The particles were governed and carried to the bed surface by the drag force in agglomerates. Gas with a high velocity stimulated colliding between the particles. In the x-direction, two cores of drag force were generated beside the spout region. For the liquid bridge and contact forces, the maximum value appeared near the walls, where the particles were thrown to both sides and collided with the walls in agglomerates. In the z-direction, the cores of the drag force increased and appeared in the spout region, where the gas velocity was high and the particle volume fraction was low. For the liquid bridge force, the cores of the high value were present in the dense region, which resulted in less active particle motions.

Therefore, the drag force mainly dominated the particle flow behaviors, and the liquid bridge force played an important role in dominating the gas-solid two-phase flow characteristics, especially near the walls with a high particle volume concentration. The contact force was more effective in the spout region with a high percentage of particles colliding.

3.4 Single-spout fluidized bed
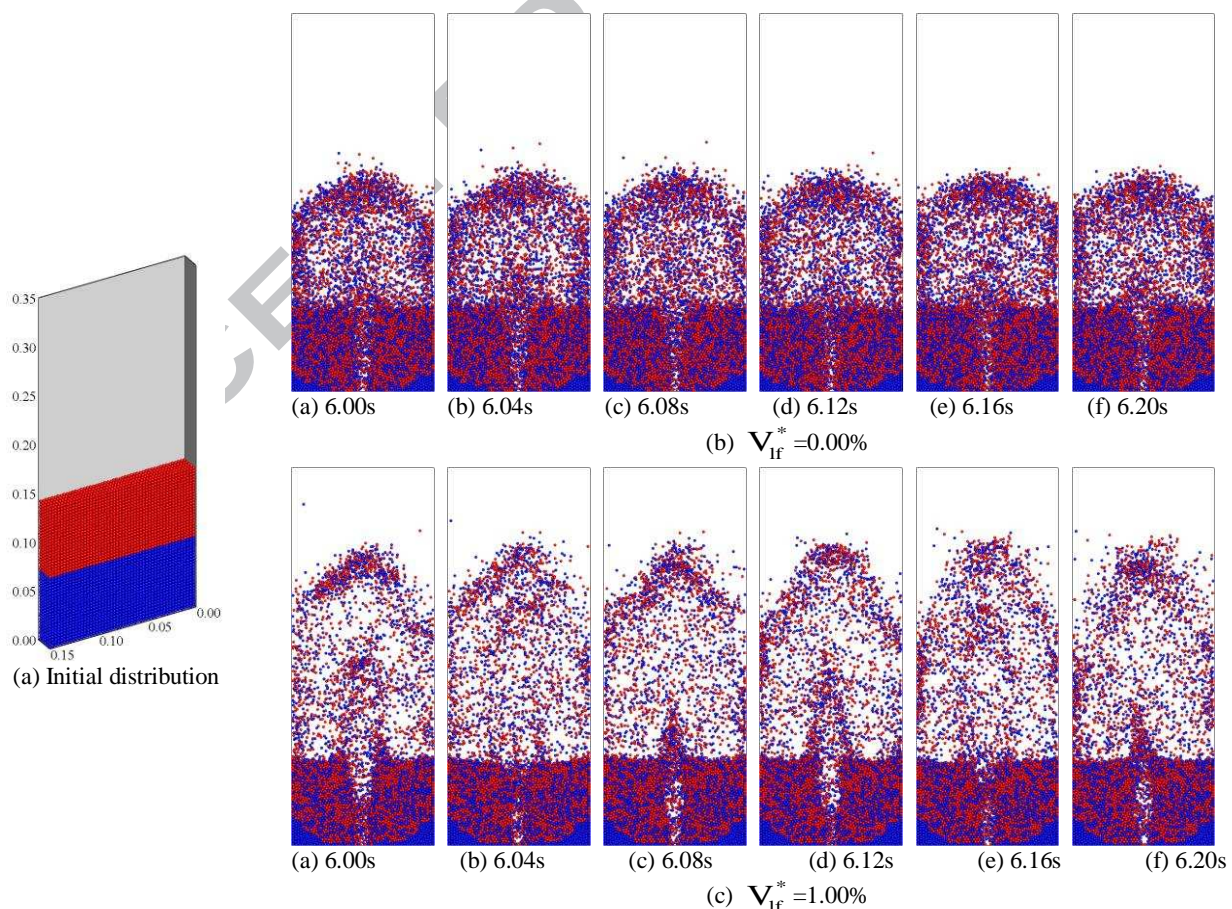
3.4.1 Particle distribution

Fig. 13 Instantaneous snapshots of the particle distribution and mixing processing in a single-spout fluidized bed

Fig. 13 shows the instantaneous snapshots of the particle distribution in a single-spout fluidized bed with a liquid content of (a) 0.00% and (b) 1.00%. The mixing process of the particles could also be obtained during the complete fluidization process. To evaluate the mixing process, the particles were marked first because all of the particles contained the same diameter and density. Initially, the particles were distributed at the bottom of the bed and divided into two groups with the same fraction. The particles were marked blue and red for the lower and upper half, respectively.

As shown in this group of figures, the particles were mixed completely in the dry and wet particle systems. The gas entered from the spouting inlet at a velocity of 43.5 m/s and formed a vertical gas channel at the bottom.

Conversely, in the wet granular system, the upper particles were thrown to the higher free space by the drag force. This phenomenon also illustrated that the gas-solid flow behaviors were influenced by the liquid between the particles. As Fig. 13 shows, the dead zones existed at the corners of the single-spout fluidized bed, especially with a flat bottom. The area and the inclined angle of the dead zones increased owing to the effect of the liquid bridge force in a wet granular system. It was difficult for the particles to flow down, and agglomerates formed easily owing to the additional cohesive force generated by the liquid between the particles.
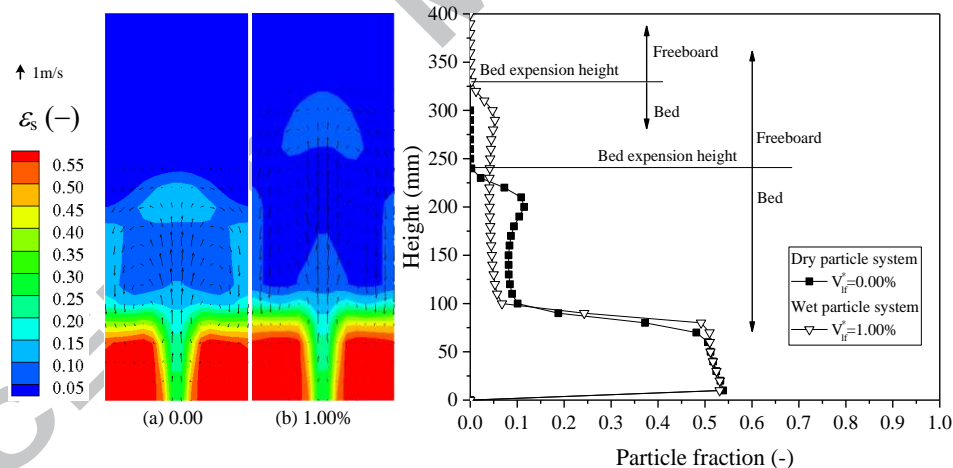
3.4.2 Expanded bed height

Fig. 14 Time-averaged particle velocity vector and expanded bed height in a single-spout fluidized bed

The expanded bed height was measured based on the variation of the cross-sectional average of the particle volume fraction along the height of the bed. Fig. 14 shows the expanded bed height for single-spout fluidized beds with and without cohesive liquid.

The profiles of the particle volume fraction were equivalent. At the heights of 100 to 250 mm and 100 to 325 mm, the annulus regions appeared for dry and wet particle systems, respectively. The expanded bed height for the dry particle system was approximately 250 mm. For the wet granular system, the expanded bed height was approximately 325 mm. The spout fluidized bed could be divided into three regions, including the spout region, fountain region, and annulus region. For the wet granular system, the heights of the annulus and spout regions were much higher than those in the dry particle system because agglomerates and gas channels were formed at the bottom. This showed that the drag force was more effective in pushing small agglomerates

upward at a high gas velocity. Thus, the expanded bed height was higher than that in the dry particle system.

3.4.3 Particle mass flux

The particle mass flux in a calculated cell is related to the average particle velocity, particle concentration, and density and was defined as,

$$\phi_i = \varepsilon_s \rho_p \overline{v}_{p,i} \tag{25}$$

The parameter ε_s is the particle concentration in a cell, and $\overline{v}_{p,i}$ is the mean particle velocity in the i direction in a cell.
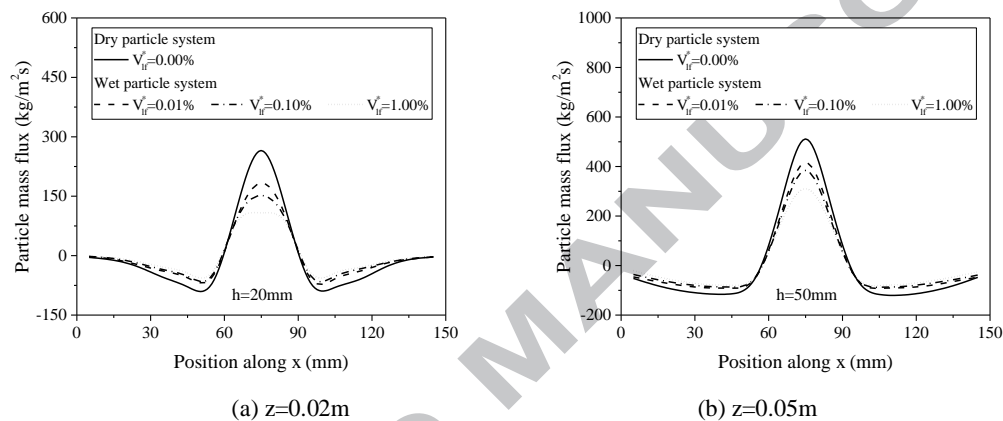

(a) z=0.02m   (b) z=0.05m

Fig. 15 Influence of liquid content on axial particle flux in a single-spout fluidized bed

Most particles flowed up in the spout regions and moved down near the walls. At the height of 20 mm, the particle mass flux varied from the peak value in the spout region and decreased to a minimum value near the walls. The particle mass flux was nearly zero at the walls. The calculated particle mass flux flowing up in the spout regions balanced with those flowing down near the walls and up in the spout region. It demonstrated that the absolute value of the particle flux declined with an increasing liquid content. The decreasing absolute value of the particle mass flux indicated that the particle movements were constrained owing to the cohesive force on the particles, and the particles were less active in wet granular systems. Fig. 15 (b) shows the particle flux distribution at a bed height of 50 mm in a single-spout fluidized bed. In contrast, the particle flux contained the same variation trend as that at a height of 20 mm. The particle mass flux increased; therefore, the particles were completely fluidized with increasing bed height.
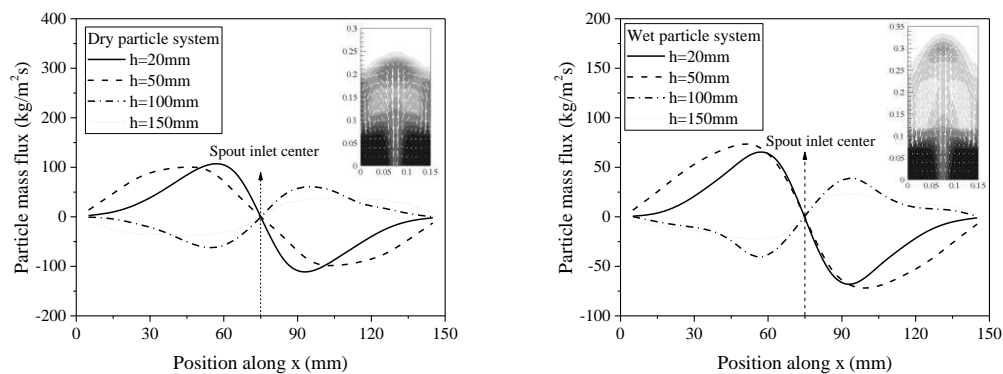
(a) Dry particle system   (b) Wet particle system

Fig. 16 Influence of liquid content on horizontal particle mass flux in a single-spout fluidized bed

Fig. 16 shows the horizontal mass flux at different heights in dry and wet particle systems. At the heights of 20 and 50 mm, the horizontal mass flux was positive for x < 75 mm and negative for x > 75 mm. This demonstrated that the particles were entrained from the annulus to the spout region at the bottom of the bed. As the spout region faded away and the bubbles ruptured with increasing bed height, the particles were pushed from the center of the bed to the annular region, as indicated by the profiles at h = 100 and 150 mm. The distribution of the horizontal particle mass flux reflected the recirculation process of the particles in the bed. The horizontal mass flux entrained into the spout region in dry particle system was higher than that in the wet particle system. Combining the axial mass particle flux distribution, the mass flux was influenced in all directions.

3.4.4 Granular temperature

According to Section 2.4, two granular temperatures were proposed by Tartan and Gidaspow owing to different oscillations of the particles. The first was the particle granular temperature representing the turbulent kinetic energy of the particles. This was one of the most important parameters for revealing the micro-scale particle turbulent movements. The second was the bubble granular temperature, which was an important physical parameter to evaluate the bubble turbulent movements. It was significant in evaluating the turbulent kinetic energy of the bubble movements. In a bubbling fluidized bed, the bubble motion phenomenon is obvious, and bubble granular temperature is suitable and important to reflect the bubble fluctuation energy. However, in a spout fluidized bed, the bubble motion is not significant, so bubble granular temperature is not suitable to describe the particle flow behaviors. Thus, the particle granular temperatures are analyzed in this work only.
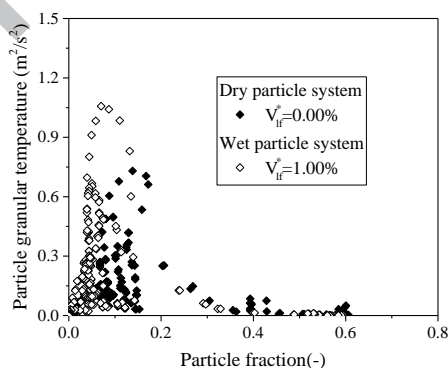

Fig. 17 Influence of liquid content on granular temperatures in a single-spout fluidized bed

From Fig. 17, the granular temperature increased and reached the peak value at a particle volume concentration of approximately 0.1. The region with a particle volume concentration within 0.1 corresponded to the fountain region and near the gas spouting inlet, where the free path of particle movement increased, and the gas velocity was high with a more effective drag force. For the wet particle system, the peak value of the particle granular temperature was slightly higher than that in the dry particle system. Combining with particle instantaneous spatial distribution, the small particle agglomerates flowed to a higher bed height because of the effect of the cohesive liquid and drag force. Therefore, the turbulent kinetic energy of the particles increased. Above all,

the increasing maximum granular temperature indicated that the fluctuation energy of the wet particles was influenced by the cohesive liquid between the particles, especially in the fountain region.

The granular temperature decreased gradually with the particle concentration when it exceeded 0.1. A high particle concentration resulted in the reduction of the free path of the particles. In dense regions, corresponding to the regions near the walls, the particles had low velocities, leading to a decline of the granular temperature. With an increasing liquid content, the particles were governed by the liquid bridge force, so the particles were less active than those in dry granular systems. In dense regions, the free path and lower velocities of the particles resulted in a decreasing granular temperature in a wet granular system.
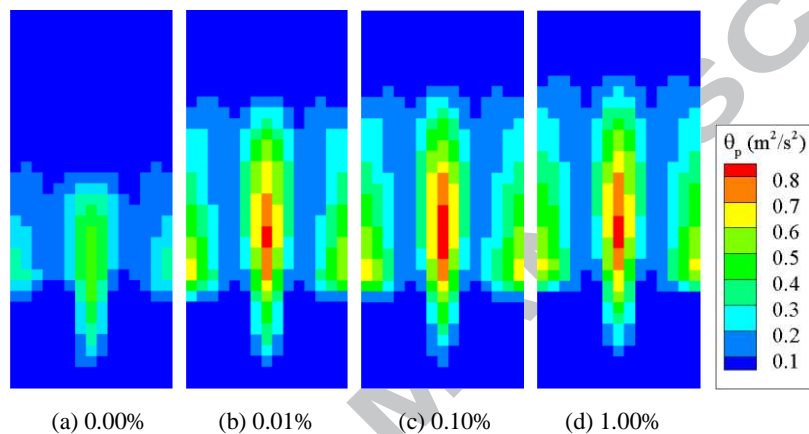

(a) 0.00%　　(b) 0.01%　　(c) 0.10%　　(d) 1.00%

Fig. 18 influence of liquid content on particle granular temperature distribution in a single spout fluidzied bed

Fig. 18 shows the cloud maps of the particle granular temperature distribution in a single-spout fluidzied bed. It is clearly observed that the distribution of the time-averaged grnaular temperature distribution is similar to that in the dry particle system. For both dry and wet particle systems, a core with a high granular temperature is generated in the spout region. The region with the high granular temperature expands gradually with an increasing of liquid content, which indicates that the fluctuation in the energy of the particles is influenced by the cohesive liquid in the wet particle systems. In addition, a pair of cores of high granular temperature appears near the walls, whose value is slightly lower than that in the spout region. This phenomenon demonstrates that the particles violently collide with walls owing to the effect of the drag force and increasing liquid bridge force. Near the dead zones, the particle motion is more gentle with less fluctuation in the energy.

3.5 Double-spout fluidized bed

3.5.1 Particle distribution

Fig. 19 shows the instantaneous snapshots of the particle distribution with a liquid content of (a) 0.00% and (b) 1.00%. The particles were marked the same as those in the single-spout fluidized bed.

As shown in this group of figures, the particles were completely mixed in the dry and wet particle systems. The gas entered from two independent spouting regions at a velocity of 40.5 m/s and formed a slanting gas passage at the bottom. The area between the two gas spouting regions and the angle of the gas passage decreased in the wet granular system. It became more difficult for the gas to flow through the particles owing to the agglomerates forming from the liquid and the particles in the bed.

At the middle of the bed height, bubbles appeared and then ruptured at the bed surface, and the upper particles were pushed to both sides and moved down along the walls. The bubble outlines from the wet particle system with a liquid content of 1% were more irregular and less visible than those in the dry particle system. In a wet granular system, the upper particles were forced to the free space in terms of agglomerates, and the particle and gas motions became violent at the bed surface. This phenomenon also illustrated that the liquid between the particles influenced the gas-solid flow behaviors. The dead zones existed in the corners of the single-spout fluidized bed. In double-spout fluidized beds, the dead zone area reduced greatly, and only a few particles were not completely fluidized in the corners. The area and the inclined angle of the dead zones increased slightly owing to the effect of the liquid bridge force in the wet granular system.
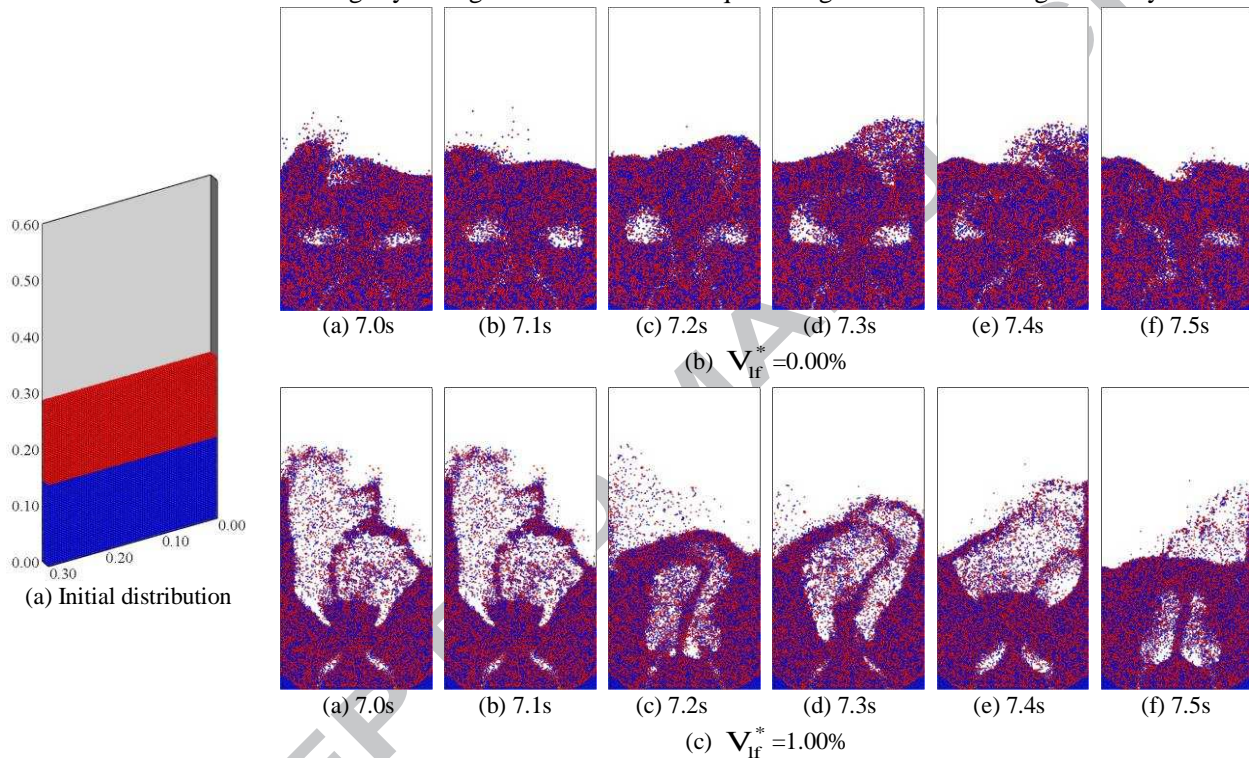

(a) 7.0s   (b) 7.1s   (c) 7.2s   (d) 7.3s   (e) 7.4s   (f) 7.5s

(b) $V_{lf}^* = 0.00\%$

(a) Initial distribution

(a) 7.0s   (b) 7.1s   (c) 7.2s   (d) 7.3s   (e) 7.4s   (f) 7.5s

(c) $V_{lf}^* = 1.00\%$

Fig. 19 Instantaneous snapshots of the particle distribution and mixing processing in a double-spout fluidized bed

3.5.2 Expanded bed height
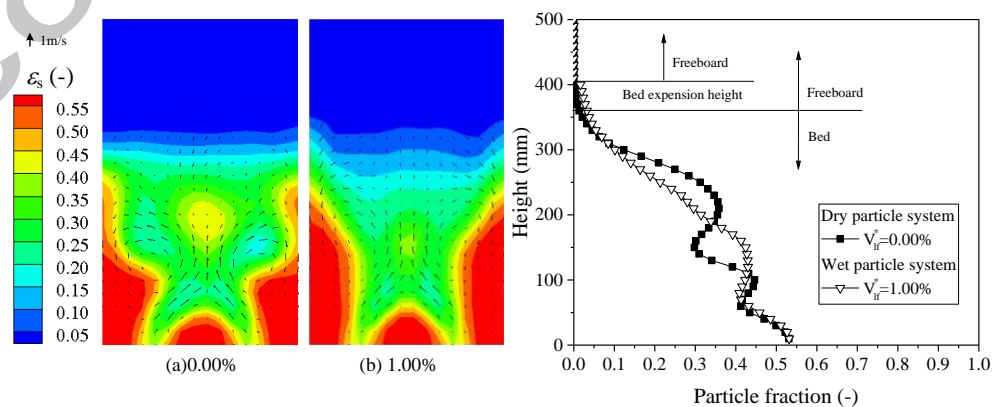

(a)0.00%   (b) 1.00%

Fig. 20 Time-averaged particle velocity vector and particle concentration in a double-spout fluidized bed

Fig. 20 shows the expanded bed height for double-spout fluidized beds with and without cohesive liquid.

The distribution profiles of the particle volume fraction were parallel below 50 mm, which corresponded to the spout region. At the heights of 50 to 350 mm and 50 to 400 mm, the annulus regions were present for the dry and wet particle systems, respectively. The expanded bed height for the dry particle system was approximately 350 mm. For the wet granular system, the expanded bed height was approximately 400 mm. Compared with the single-spout fluidized bed, the fountain region is not obvious. For the wet granular system, the heights of the annulus region were slightly higher than those in the dry particle system under the effect of the liquid bridge force and the drag force. This was similar to the phenomenon shown in the single-spout fluidized bed.

3.5.3 Particle mass flux

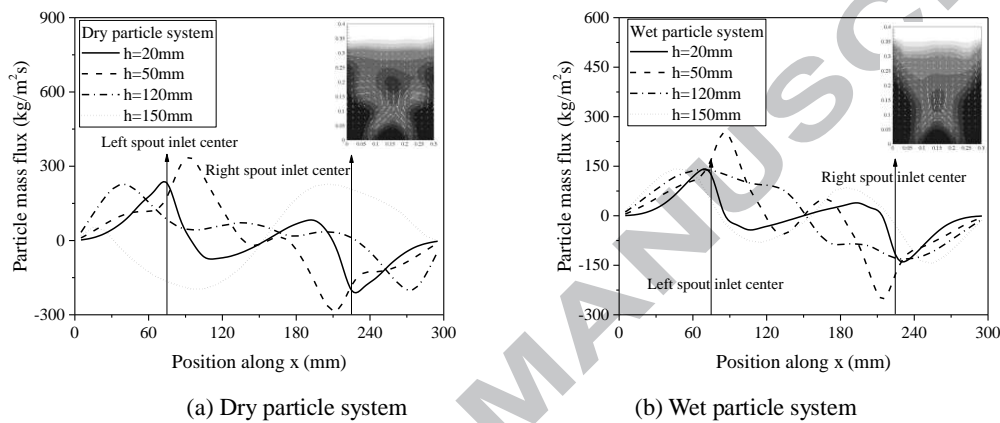(a) Dry particle system   (b) Wet particle system

Fig. 21 Influence of liquid content on horizontal particle mass flux in a double-spout fluidized bed

Fig. 21 shows the influence of the liquid content on the lateral particle mass flux at different heights. The distribution in the double-spout fluidized bed is different from that in the single-spout fluidized bed. In the dry particle system, the distributions of the lateral particle mass flux are symmetrical about the center at the different heights.

At the height of 20 mm, the lateral particle mass flux is positive for $x < 90$ mm and negative for $x > 210$ mm, indicating that the particles are entrained from the annulus to the spout region. Furthermore, the lateral particle mass flux is positive for $150 < x < 210$ mm and negative for $90 < x < 150$ mm, which forms a small annulus region and demonstrates that the particles flow from the dead zones (between the two spout regions) to the spout region. The particles move from the two regions to the spout region, which is different from the results of the single-spout fluidized bed.

With increasing bed height, the particles are gradually completely fluidized and the dead zones between the two gas channels disappeared gradually. At the bed height of 50 mm, the small annulus region vanished, and the distribution of the lateral particle mass flux is similar to that in the single-spout fluidized bed.

At the bed height of 120 mm, the peaks of the lateral particle mass flux are close to the side walls compared with the distribution at lower heights and the middle annulus region vanishes completely. At the bed height of 150 mm, the distribution of the particle mass flux is reversed, i.e., it is positive for $x > 150$ mm and negative for $x < 150$ mm. This phenomenon demonstrates that the particles flow from the spout to the annulus region. As mentioned above, the particles circulate periodically in the spouted fluidized bed.

In the wet granular system with a liquid content of 1.00%, at the bed heights of 20 and 50 mm, the horizontal particle mass flux distribution is similar to that in the dry particle system with a smaller particle mass flux. The reason for this is that the particles are much harder to be fluidized

owing to the presence of the cohesive liquid bridge force in the wet granular system. At the bed height of 150 mm, the lateral particle mass flux is different from that in the dry particle system. The particles form agglomerate under the effect of the cohesive liquid, because of which the distribution of the lateral particle mass flux is more violent than that in the dry particle system.
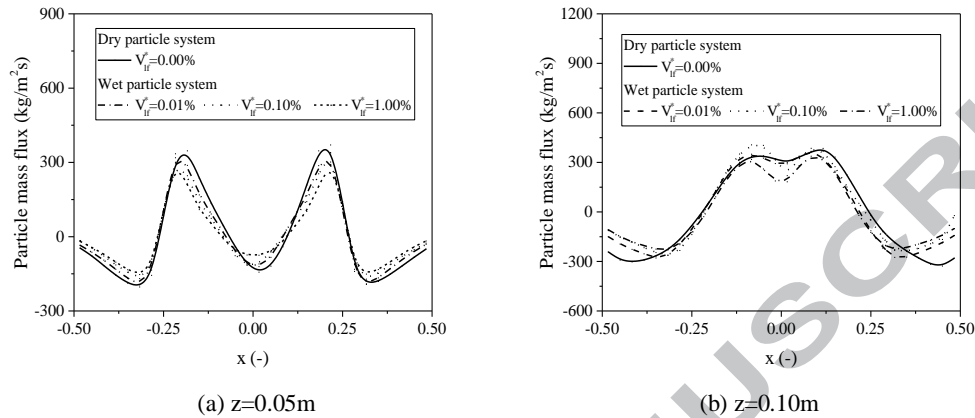

(a) z=0.05m   (b) z=0.10m

Fig. 22 Influence of liquid content on axial particle flux in a double-spout fluidized bed

Fig. 22 shows the influence of the liquid content on the axial particle mass flux at different heights. Most of the particles flowed up in the two spout regions, and they moved down near the walls and between the two gas spouting regions. At a height of 50 mm, the particle mass flux varied from the two peak values in the spout regions and decreased to a minimum value in the bed center and near the walls. The particle mass flux was nearly zero at the walls. However, the calculated particle mass flux flowing up in the spout regions balanced with those flowing down near the walls and between the spout regions demonstrating that the absolute value of the particle flux declined with increasing liquid content. This phenomenon was similar to that shown in the single-spout fluidized bed. Fig. 18(b) shows the particle flux distribution at a bed height of 100 mm in the double-spout fluidized bed. The particle flux had the same variation trend as that at the height of 50 mm. However, the particles between the spout regions were more active and easier to be driven to move upwards by the spout gas. Near the walls, the particle flux value decreased instead of declining to zero. This illustrated that the particles were completely fluidized with increasing bed height.
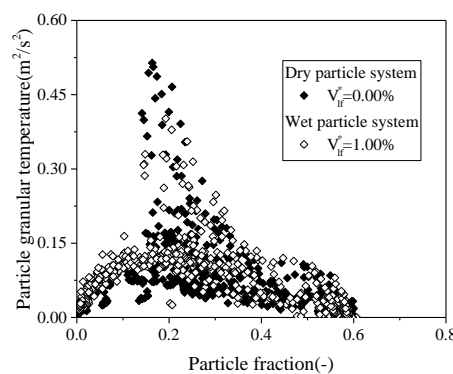
3.5.4 Granular temperature

Fig. 23 Influence of liquid content on particle granular temperatures in a double-spout fluidized bed

Fig. 23 shows the particle granular temperature in a double spout fluidized bed. Compared

with the single-spout fluidized bed, the distribution of granular temperatures is similar. However, the values of the particle granular temperatures were higher than those in the double-spout fluidized bed. When combining the profiles of the pressure drop, the particles were more active and fluidized completely in the single-spout fluidized bed; therefore, the turbulence of granular was more violent in the single-spout fluidized bed. In addition, the granular temperature in the wet granular system is slightly lower than that in the dry particle system. This is different from the single-spout fluidized bed results because the fountain region and the gas channel are not present in the double-spout fluidized bed. More particles were fluidized. Therefore, the turbulence of particles was less active than that in the single-spout fluidized bed. However, the granular temperatures decreased with increasing liquid contents owing to the influence of the cohesive liquid.

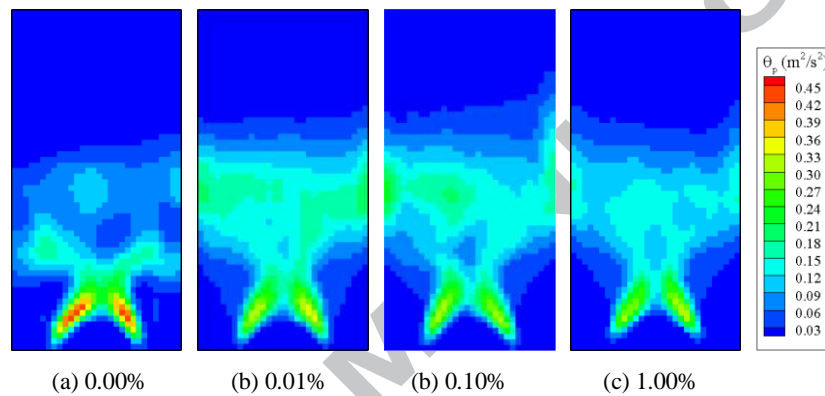(a) 0.00%   (b) 0.01%   (b) 0.10%   (c) 1.00%

Fig. 24 Influence of liquid content on time-averaged particle granular temperature

Fig. 24 shows the cloud map of granular temperature distribution in a double spout fluidzied bed. It is obvious to obtain that the distribution of grnaular temperature distribution is similar and the value of the granular temperature is slightly higher than that in the dry particle system. For both the dry and wet particle systems, a pair of inclining high particle granular temperatures is generated in the spout regions, which is similar to the phenomenon in the single-spout fluidized bed. Because more particles have to be fluidized, particles are less active in the double-spout fluidized bed. Additionally, the distribution of the particle granular temperature near the walls is different from that in the single-spout fluidized bed. According to the instantaneous particle spatial distribution, it is obvious to obtain that the particles are less active to collide with the side walls in the double-spout fluidized bed. Thus, the particle granular temperatures are lower in the double-spout fluidized bed.

3.6 Analysis of solid circulation

A measure of the solid circulation rates was calculated in this study using the counter-current model proposed by Geldart et al. (1986). The net solid circulation rate was given by the following equation,

$$\left|\vec{m}_{tot}\right| = \rho_p \times (\varepsilon_{s,b}) \times (f_{r_{neg}}) \times (\left|\vec{v}_{neg,avg}\right|) \times (A_d) \tag{26}$$

where $\varepsilon_{s,b}$ represents the bulk solid fraction of the bed, which was calculated based on the expanded height of the bed. Besides, $f_{r_{neg}}$, A_d, and $\left|\vec{v}_{neg,avg}\right|$ represent the fraction of the bed moving downward, the area of the distributor plate, and the average magnitude of the downward velocity of the particles in the bed, respectively.

Fig. 25 shows the solid circulation rate, which demonstrated that the solid circulation rate in a single-spout fluidized bed was higher than that in a double-spout fluidized bed under the same condition. This phenomenon was consistent with the experimental results from Agarwal et al. (2012) and simulation results from Ded et al. (2012). The solid circulation rate values were compared at different liquid contents. As observed from Fig. 25, the solid circulation rate decreased sharply when the liquid content increased from 0.00% to 0.01% and 0.10%. Furthermore, the change became stable from 0.01% to 1.00%. This showed that the presence of the cohesive liquid had a significant impact on the particle flow behavior and the solid circulation. When combining the distribution of the particle mass flux, the solid circulation rate decreased with decreasing particle mass flux and increasing liquid content.
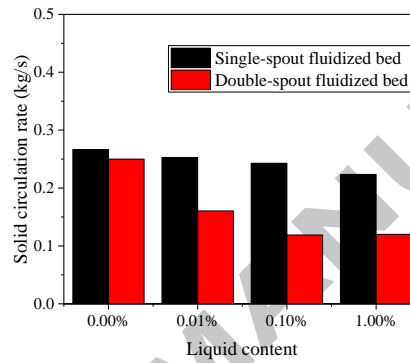

Fig 25 Solid circulation rate with change in liquid content for single and double spouted fluidized bed

3.7 Analysis of the mixing characteristics

A mixing index was used to explain the mixing processes of the particles in spout fluidized beds. The well-known Lacey index (Lacey et al., 1954) is given by the following equation,

$$M = \frac{\sigma_0^2 - \sigma}{\sigma_0^2 - \sigma_R^2} \tag{27}$$

where σ_0^2 is the variance of the completely separated system, and σ_R^2 is the variance of the completely mixed system, and σ^2 is the variance of the mixture between the fully random and completely segregated mixtures and is defined as,

$$\sigma^2 = \frac{1}{N-1} \sum_{i=0}^{N} \left(c_i - \overline{c} \right) \tag{28}$$

here, N is the number of cell for statistic; c_i is the local fraction of the sample particles, and $\overline{c}$ is the average fraction of the sample particles.

The influence of the cohesive liquid on the mixing index is shown in Fig. 21. The liquid content increased to 1.00% in the wet granular system. According to the distribution of mixing, the Lacey mixing index remained a constant after 4 s for the dry and wet particle systems. Thus, the mixing processes reached a dynamic balance. The mixing equilibrium decreased from 0.838 to 0.687 for the dry and wet particle systems, respectively. The particle flow behaviors were influenced by the liquid bridge force, which corresponded to the increasing dead zones near the corner, as shown in Fig. 12.
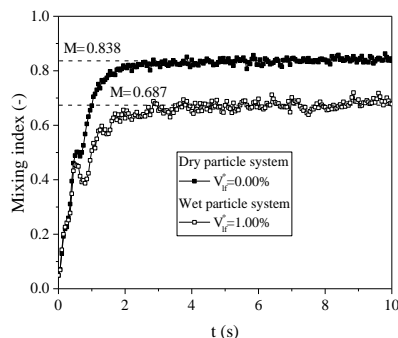
Fig 26 Influence of presence of cohesive liquid on the mixing characteristic in a single-spout fluidized bed

According to the distribution of the Lacey mixing index, particles are mixed more completely in the double-spout fluidized bed, as shown in Fig. 27 (a), as a result of which the average particle collision percentage also increases as Fig. 27 (b) shown. This phenomenon demonstrates that the spouted fluidized bed with more gas inlets can stimulate the mixing process, and multiple-spout fluidized beds can provide more space for mass and heat transfer.

Furthermore, the influence of the liquid content is analyzed. With an increasing of liquid content, the mixing index was reduced with a more effective liquid bridge force. It can be explained that liquid bridge force increases the resistance of particle motion, and the mixing index decreases. However, a more effective liquid bridge force led to a higher particle colliding percentage owing to the closer distance between the particles.

(a) Mixing index   (b) Percentage of colliding particles
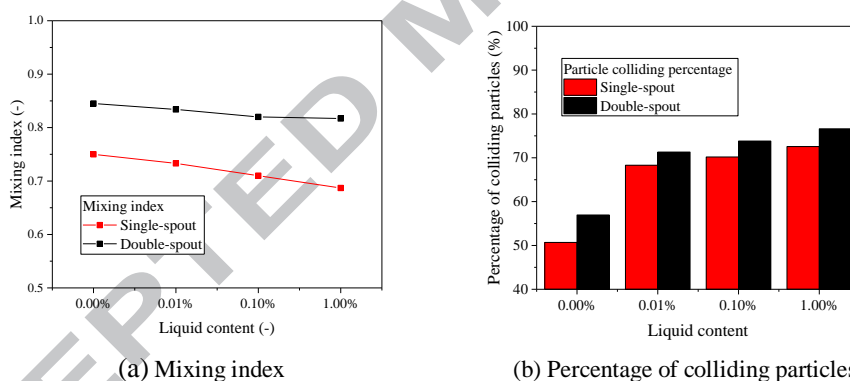
Fig. 27 Influence of liquid content on average percentage of colliding particles and mixing index in multiple spouted fluidized beds

Above all, all the particle flow behaviors are analyzed and summarized in Table 6. It is clear that the double-spout fluidized bed can provide more space for mass and momentum exchange. First, the circulation rate reflects the particle circulation characteristics. In this work, for the double-spout fluidized bed, the spout and fluidization gas velocities are similar, while the circulation rate is slightly lower as more particles have to be fluidized. However, this phenomenon is more suitable for particles colliding with each other and mixing more completely. Thus, the mixing index and particle colliding percentage are higher in the double-spout fluidized bed demonstrating that a spouted fluidized bed with more gas inlets is beneficial for particle mixing and important for industrial processing.

Table 6 A comparison of particle flow behavior in single and double spout fluidized bed.

Parameter	Comparison
Circulation rate	Single > double
Mixing index	Single < double

Particle colliding percentage	Single < double

4 Conclusions

In this study, a modified DEM was applied to investigate the hydrodynamic characteristics of dry and wet particles. Simulations of the dry and wet particles were conducted in single- and double-spouted fluidized beds. Different liquid contents were applied for a further investigation on the particle flow behaviors in a wet granular system. A force analysis of the wet particles was conducted. A comparison of the particle mass flux distribution, granular temperature, and pressure drop was conducted to determine the effect of the liquid on the particle flow characteristics in the dry and wet particle systems. Furthermore, a comparison of the particle flow behaviors in single-spout and double-spout fluidized beds was carried out.

Overall, the modified DEM method with the liquid bridge module was capable of describing the gas-solid flow behaviors. Model verification and model validation have been applied to demonstrate the accuracy and rational of the simulation method. The comparison of drag force model and independence test are applied in this work. Besides, the simulation results with a liquid content of 1% showed good agreement with the experimental data from Buijtenen et al. In a wet granular system, the effect of the liquid bridge force was evident at the bed surface and near the walls, where the particles formed agglomerates under the effect of the liquid bridge force.

To explain the effect of the cohesive liquid, a force analysis was carried out. The drag force primarily dominated the particle flow behavior. The liquid bridge force had an effect on the dense region. The liquid bridge force was ten times larger than the force of gravity and influenced the particle flow behavior in the wet granular system.

In addition, the influence of the liquid contents on the particle flow behavior was investigated. The absolute value of the particle mass flux decreased owing to a more effective liquid bridge force. This indicated that the particle motions were constrained because of the cohesive liquid between the particles. With increasing liquid content, the pressure drop fluctuation and the expanded bed height increased, and the average values of the pressure drop decreased. This indicated that the additional liquid bridge force was overcome by the gas flowing up to the bed surface. Moreover, the distribution of the particle and bubble granular temperatures illustrated that the fluctuation energy of the particles and bubbles was reduced with a decreasing free path and particle velocity when the liquid content increased.

Furthermore, a comparison of the particle flow behaviors in single-spout and double-spout fluidized beds was conducted. We found that the solid circulation rate decreased with an increasing number of spouting inlets and liquid contents. Particularly, the colliding percentage of the particles was slightly higher than that in the double-spout fluidized bed. However, the colliding percentage between the particles and the walls in a single-spout fluidized bed was slightly higher than that in the double-spout fluidized bed. Moreover, the mixing index was higher than that in the double-spout fluidized bed with more sufficient colliding. Therefore, the double-spout fluidized bed could provide more space for particle mass and heat transfer and could be used for designing the chemical reactor.

Acknowledgements

References

[1] Van Buijtenen M. S., Van Dijk W. J., N. G., Leadbeater, T., Parker, D. J., 2011. Numerical and experimental study on multiple-spout fluidized beds, Chem. Eng. Sci. 66(11), 2368-2376.

[2] Ye B., Lim C. J., Grace J. R..1992. Hydrodynamics of spouted and spout-fluidized beds at high temperature, Can. J. Chem. Eng. 70(5): 840-847.

[3] Sutkar V. S., Deen N. G., Kuipers J. A. M., 2013. Spout fluidized beds: Recent advances in experimental and numerical studies, Chem. Eng. Sci. 86, 124-136.

[4] Van Buijtenen M. S., Börner M., Deen N. G., Heinrich, S., Antonyuk, S., Kuipers, J. A. M., 2011. An experimental study of the effect of collision properties on spout fluidized bed dynamics, Powder Technol. 206(1), 139-148.

[5] Luo K., Yang S., Zhang K., Fang, M., Fan, J., 2013. Particle dispersion and circulation patterns in a 3D spouted bed with or without draft tube. Ind. Eng. Chem. Res. 52(28), 9620-9631.

[6] Duarte C. R., Olazar M., Murata V. V., Barrozo, M. A. S., 2009. Numerical simulation and experimental study of fluid–particle flows in a spouted bed, Powder Technol. 188(3), 195-205.

[7] Filla M., Massimilla L., Vaccaro S., 1983. Gas jets in fluidized beds and spouts: a comparison of experimental behavior and models, Can. J. Chem. Eng. 61(3), 370-376.

[8] Zhong W., Zhang M., 2005. Pressure fluctuation frequency characteristics in a spout-fluid bed by modern ARM power spectrum analysis, Powder Technol. 152(1), 52-61.

[9] Link J., Zeilstra C., Deen N., Kuipers, H., 2004. Validation of a discrete particle model in a 2D spout-fluid bed using non-intrusive optical measuring techniques, Can. J. Chem. Eng. 82(1), 30-36.

[10] Kawaguchi T., Sakamoto M., Tanaka T., Tsuji, Y., 2000. Quasi-three-dimensional numerical simulation of spouted beds in cylinder, Powder Technol. 109(1), 3-12.

[11] Zhang Y., Jin B., Zhong W., 2010. DEM simulation of particle mixing in flat-bottom spout-fluid bed. Chem. Eng. Res. and Des. 88(5), 757-771.

[12] Yang, S., Luo, K., Fang, M., Zhang, K., Fan, J., 2014. Parallel CFD–DEM modeling of the hydrodynamics in a lab-scale double slot-rectangular spouted bed with a partition plate, Chem. Eng. J. 236, 158-170.

[13] Deb S., Tafti D., 2014. Investigation of flat bottomed spouted bed with multiple jets using DEM–CFD framework, Powder Technol. 254, 387-402.

[14] Wang X., Jin B., Wang Y., Hu, C., 2015. Three-dimensional multi-phase simulation of the mixing and segregation of binary particle mixtures in a two-jet spout fluidized bed, Particuology 22. 185-193.

[15] Saidi M., Tabrizi H. B., Grace J. R., Lim, C. J., 2015. Hydrodynamic investigation of gas-solid flow in rectangular spout-fluid bed using CFD-DEM modeling, Powder Technol. 284, 355-364.

[16] Khadilkar A., Rozelle P. L., Pisupati S. V., 2014. Models of agglomerate growth in fluidized bed reactors: Critical review, status and applications, Powder Technol. 264, 216-228.

[17] Zielinska M., Markowski M., 2007. Drying behavior of carrots dried in a spout–fluidized bed dryer, Drying Technol. 25(1), 261-270.

[18] Liao C. C., Hsiau S. S., 2010. Experimental analysis of dynamic properties in wet sheared granular matter, Powder Technol. 193, 222-229.

[19] Chou S. H., Hsiau S. S., 2011. Experimental analysis of the dynamic properties of wet granular matter in a rotating drum, Powder Technol. 214, 491-499.

[20] Pain C. C., Mansoorzadeh S., De Oliveira C. R. E.,2001. A study of bubbling and slugging fluidised beds using the two-fluid granular temperature model, Int. J. Multiphase Flow. 27(3), 527-551.

[21] Lu B., Wang W., Li J., 2009. Searching for a mesh-independent sub-grid model for CFD simulation of gas–solid riser flows, Chem. Eng. Sci. 64(15), 3437-3447.

[22] Wang J., Van der Hoef M. A., Kuipers J. A. M., 2009. Why the two-fluid model fails to predict the bed expansion characteristics of Geldart A particles in gas-fluidized beds: a tentative answer, Chem. Eng. Sci. 64(3), 622-625.

[23] Tsuji Y., Kawaguchi T., Tanaka T., 1993. Discrete particle simulation of two-dimensional fluidized bed, Powder Technol. 17, 79–87.

[24] Cundall P. A., Strack O. D. L., 1979. A discrete numerical model for granular assemblies, Geotechnique 29(1), 47-65.

[25] Chang W., Hsieh S., Yang F., Chen C., 2008. Discrete element simulation of collision-rich dynamics of wet granular flows down an inclined channel, Tsinghua Sci. Technol. 13, 90-95.

[26] Teufelsbauer H., Wang Y., Pudasaini S. P., Borja R. I., Wu W., 2011. DEM simulation of impact force exerted by granular flow on rigid structures, Acta Geotech. 6, 119-133.

[27] Xu Y., Xu C., Zhou Z., Du J., Hu D., 2010. 2D DEM simulation of particle mixing in rotating drum: A parametric study, Particuology 8, 141-149.

[28] Arntz M., Den Otter W. K., Briels W. J., Bussmann P. J. T., Beeftink H. H., Boom R. M., 2008. Granular mixing and segregation in a horizontal rotating drum: a simulation study on the impact of rotational speed and fill level, AIChE J. 54, 3133-3146.

[29] Jia D., Cathary O., Peng J., Bi X. , Lim C., 2015. Fluidization and drying of biomass particles in a vibrating fluidized bed with pulsed gas flow, Fuel Process. Technol.

[30] Zhuang Y., Chen X. , Luo Z., Xiao J., 2014. CFD–DEM modeling of gas–solid flow and catalytic MTO reaction in a fluidized bed reactor, Comput. Chem. Eng. 60, 1-16.

[31] Limtrakul S., Boonsrirat A., Vatanatham T., 2004. DEM modeling and simulation of a catalytic gas–solid fluidized bed reactor: a spouted bed as a case study, Chem. Eng. Sci. 59(22), 5225-5231.

[32] Zhao X. L., Li S. Q., Liu G. Q., 2008. DEM simulation of the particle dynamics in two-dimensional spouted beds, Powder Technol. 184(2), 205-213.

[33] Jajcevic D., Siegmann E., Radeke C., 2013. Large-scale CFD–DEM simulations of fluidized granular systems, Chem. Eng. Sci. 98, 298-310.

[34] Anderson T. B., Jackson R., 1967. Fluid Mechanical Description of Fluidized Beds. Equation of Motion, Ind. Eng. Chem. Fundam. 6(4), 527-539.

[35] Zhou Y. C., Wright B. D., Yang R. Y., Xu, B. H., Yu, A. B., 1999. Rolling friction in the dynamic simulation of sandpile formation, Physica A 269(2), 536-553.

[36] Wang X. L., Li J. C., 2014. Simulation of triaxial response of granular materials by modified DEM, Sci. China Phys. Mech. 57(12), 2297-2308.

[37] Hosn R. A., Sibille L., Benahmed N., Chareyre, B., 2017. Discrete numerical modeling of loose soil with spherical particles and interparticle rolling friction, Granul. Matter, 19(1), 4.

[38] Gidaspow D., 1994. Multiphase Flow and Fluidization: Continuum and Kinetic Theory Descriptions. New York: Academic Press.

[39] Johnson K. L., 1985. Contact Mechanics Cambridge: Cambridge University Press.

[40] Morris A. B., Pannala S., Ma Z., Hrenya, C. M., 2016. Development of soft-sphere contact models for thermal heat conduction in granular flows, AIChE J., 62(12), 4526-4535.

[41] Girardi M., Radl S., Sundaresan S., 2016. Simulating wet gas–solid fluidized beds using coarse-grid CFD-DEM, Chem. Eng. Sci. 144, 224-238.

[42] Israelachvili J. N., 1992. Intermolecular and Surface Forces, San Diego: Academic Press.

[43] Bird R. B., 1960. WE stewart and EN Lightfoot, Transport phenomena.

[44] Adams M. J., Edmondson B., 1987. Forces between particles in continuous and discrete liquid media, Tribology in Particulate Technol.

[45] Lian G., Thornton C., Adams M. J., Thornton C., 1996. Elastohydrodynamic collisions of solid spheres. J. Fluid Mech. 331, 141-152.

[46] Lian G., Thornton C., Adams M. J., 1993. A theoretical study of the liquid bridge forces between two rigid spherical bodies, J. Colloid Interf. Sci. 163, 138-147.

[47] Pritchett J. W., Blake T. R., Garg S. K.,1987. A numerical model of gas fluidized beds, AIChE Symp. Ser. 74(176), 134.

[48] Beetstra R., Van der Hoef M. A., Kuipers J. A. M., 2007. Drag force of intermediate Reynolds number flow past mono-and bidisperse arrays of spheres, AIChE J. 53, 489-501.

[49] Koch D. L., Hill R. J., 2001. Inertial effects in suspension and porous-media flows, Annu. Rev. Fluid Mech. 33, 619–647.

[50] Tartan M., Gidaspow D., 2004. Measurement of granular temperature and stresses in risers, AIChE J. 50, 1760-1775.

[51] Jung J., Gidaspow D., Gamwo I. K., 2005. Measurement of two kinds of granular temperatures, stresses, and dispersion in bubbling beds, Ind. Eng. Chem. Res. 44, 1329-1341.

[52] Kuo H. P., Knight P. C., Parker D. J., Tsuji Y., Adams M. J., Seville J. P. K., 2002. The influence of DEM simulation parameters on the particle behaviour in a V-mixer, Chem. Eng. Sci. 57(17), 3621-3638.

[53] Guédon G. R., Besagni G., Inzoli F., 2017. Prediction of gas–liquid flow in an annular gap bubble column using a bi-dispersed Eulerian model, Chem. Eng. Sci. 161, 138-150.

[54] Boyce C. M., Ozel A., Rice N. P., Rubinstein, G. J., Holland, D. J., Sundaresan, S., 2016. Effective particle diameters for simulating fluidization of non-spherical particles: CFD-DEM Models vs. MRI Measurements, AIChE J.

[55] Landi G., Barletta D., Poletto M., 2011. Modelling and experiments on the effect of air humidity on the flow properties of glass powders, Powder Technol. 207(1), 437-443.

[56] Geldart D., 1986. Gas Fluidization Technology, Wiley, Chichester (New York).

[57] Agarwal G., Lattimer B., Ekkad S., Vandsburger U., 2012. Experimental study on solid circulation in a multiple jet fluidized bed, AIChE J. 58(10), 3003–3015.

[58] Lacey P. M. C., 1954. Developments in the theory of particle mixing, J. Chem. Technol. Biot. 4(5), 257-268.

Highlights

A modified DEM (Discrete Element Method) approach has been applied.

A force analysis of wet particles in single and double spout fluidized bed has been performed.

The particle flow behaviors in single and double spout fluidized bed have been investigated with cohesive liquid.

The effect of liquid contents on gas-solid hydrodynamic characteristics has been found.

The relative humidity of air has been considered to validate the accuracy of the model.